Connectivity and computations in higher-order olfactory neurons in Drosophila

Dissertation Advisor: Professor Rachel I. Wilson Mehmet Fişek

Connectivity and computations in higher-order olfactory neurons in *Drosophila*

Abstract

Understanding how odors are encoded in the brain is of fundamental importance to neurobiology. The first two stages of olfactory information processing have been relatively well studied in both vertebrates and invertebrates. However, the organizational principles of higher order olfactory representations remain poorly understood. Neurons in the first relay of the olfactory system segregate into glomeruli, each corresponding to an odorant receptor. Higher-order neurons can receive input from multiple glomeruli, but it is not clear how they integrate their inputs and generate stimulus selectivity.

In the fruitfly *Drosophila melanogaster* and other insects, there are two higher-order olfactory brain regions—the lateral horn and the mushroom body. These areas are thought to be functionally specialized in how they encode odorants and what mechanisms they use. One proposal suggests that the mushroom body performs associative computations and underlies olfactory learning capabilities, whereas the lateral horn is proposed to perform stereotyped computations that underlie unlearned odor-driven behaviors. While the mushroom body has received considerable attention, we know little about how lateral horn neurons (LHNs) integrate information across glomeruli and how they respond to odorants.

Here we show that LHNs receive input from sparse and stereotyped combinations of glomeruli that are coactivated by odors, and that certain combinations of glomeruli are

over-represented. We show that one morphological LHN type is broadly tuned and sums input from multiple glomeruli. These neurons have a broader dynamic range than their individual glomerular inputs do. By contrast, a second morphological type is narrowly tuned and receives prominent odor-selective inhibition through both direct and indirect pathways. We show that this wiring scheme confers increased selectivity. Our findings show that the connectivity and stimulus selectivity of LHNs contrasts with the properties of mushroom body neurons. These differences support the notion that the lateral horn performs stereotyped computations that could mediate unlearned behaviors. Our findings also show that LHNs perform a greater diversity of computational operations than previously thought. We also present, in chapter four, new techniques we are developing for comprehensive and high-throughput mapping of the inputs to individual lateral horn neurons.

Table of Contents

List of Figures

List of Tables

Acknowledgements

First and foremost, I would like to thank my advisor Rachel Wilson for her unlimited support, guidance and patience. I've relied on Rachel's compassion and generosity for several years, and I owe her a tremendous amount for the caring she has shown. Rachel's scientific vision and clarity shaped this project, and are constant sources of inspiration for me.

I have had the pleasure of working with many amazing people in the Wilson lab and I would like to thank all of them for creating an exciting, supportive and stimulating work environment. I owe many thanks to Vikas Bhandawat, who was very generous with his time and provided invaluable instruction when I was getting started in the lab. I would like to thank Joey Zhou for late night company in the lab, Brendan Lehnert for helpful self improvement advice, Quentin Gaudry for his never ending cheer, Nathan Gouwens, Joe Bell, Wendy Liu, Allison Baker, and Tony Azavedo for their support and friendship over the years. I would like to thank Emre Yaksi, Hokto Kazama, Betty Hong and Kathy Nagel for their very thoughtful scientific advice and friendship. I would like to thank Willie Tobin and James Jeanne for their friendship of course and for tolerating working more closely with me on team lateral horn.

I am grateful to Arpiar Saunders, Ben Ewen-Campen and John Tuthill for their openness, their friendship, their support and for sharing with me their enthusiasm for biology.

I thank the faculty who served on my dissertation advisory committee for their advice and support over the years: Rick Born, Bruce Bean, Markus Meister and Bob Datta. I thank Bruce and Markus for allowing me to rotate in their labs.

I thank Matthew Banghart for his excellent advice pertaining to the design of the uncaging experiments described in Chapter 4. Those experiments would not be possible without his input.

I am grateful to the Howard Hughes Medical Institute for fellowship support.

I'm also very grateful for the support and guidance of my first mentor, Eve Marder, who gave me the love of physiology, and the confidence to explore.

My wonderful girlfriend Emine provided me with love, support and perspective during some of my toughest times and I am hugely grateful for her companionship. Her passion for her work and her beautiful perspective has had an inspiring effect on my life and my work.

Lastly I thank my parents, Güler and Hamit, and my sister, Emine. They have given me everything I have, and are my source of strength and conscience. Thanks to their immeasurable efforts and their presence, I lead a truly privileged and wonderful life. In everything I do, I hope to make them proud.

Attributions

Chapters 1, 2, 3 and 5 are modified versions of, or include modified sections of an article published as:

M. Fişek and R.I. Wilson. Stereotyped connectivity and computations in higher-order olfactory neurons. *Nature Neuroscience* **17**, 280-288 *(2014)*.

I collected and analyzed all data presented in this dissertation. The text was written together with my advisor, Rachel I. Wilson. Chapter 4 presents unpublished work.

Chapter 1.

Introduction

Volatile chemicals in the environment are a rich source of information for living organisms. Odors carry signals about food, sexual partners, and potential dangers. Thus, the sense of smell is central to the ecology of many organisms, and understanding how odors are encoded in the brain is of fundamental importance to neurobiology. The first two stages of olfactory information processing have been relatively well studied in both vertebrates and invertebrates. In comparison, the principles of higher order olfactory information processing remain poorly understood in all species. Specifically, we would like to know how higher order olfactory neurons respond to odorants, whether they are selective for particular features of olfactory stimuli, and what mechanisms support the generation of stimulus selectivity.

1.1 Stimulus selectivity in the early olfactory system.

It is generally thought that the stimulus selectivity of a sensory neuron is generated in part by the pattern of synaptic connections it receives. Simple cells in primary visual cortex are a well-understood example of this: orientation selectivity is generated largely by selective summation over thalamic neurons with co-linear receptive fields[1–3]. In olfaction, a similar level of understanding of the relationship between connectivity and selectivity exists only at the early stages of information processing.

In both vertebrates and invertebrates the odorant selectivity of a primary olfactory neuron is determined by the particular type of olfactory receptor it expresses[4–7]. All

primary neurons that express the same type of receptor send projections into the brain and converge onto a small region of neuropil called a glomerulus. As a general rule each glomerulus corresponds to one particular odorant receptor. In vertebrates, ~1000 glomeruli reside in a region termed the Olfactory Bulb (OB). In invertebrates the homologous region is termed the Antennal Lobe (AL) and contains ~50 glomeruli[8].

In *Drosophila,* secondary neurons in the AL, called Projection Neurons (PNs), arborize mainly in a single glomerulus. These uniglomerular PNs are cholinergic. However a minority of PNs are multiglomerular and GABAergic[9–11]. The main determinant of the odorant selectivity of a PN is the identity of the glomerulus it arborizes in, and therefore the identity of the corresponding odorant receptor[12–14]. Some glomeruli are innervated by multiple PNs, and the odorant selectivity of these "sister" PNs is highly correlated[15].

Lateral inter-glomerular interactions in the Antennal Lobe alter the odorant selectivity conferred to glomeruli by their feedforward inputs. Both excitatory and inhibitory interactions exist.[16,17] However the dominant lateral force appears to be inhibitory, in that removal of lateral inputs generally disinhibits odorant responses[17]. In agreement with this finding, incorporating global (spatially unselective) lateral inhibition into a model of PN odorant responses, in the form of divisive normalization, accounts for a large fraction of the variance unaccounted for by feedforward processing[18]. While current models do fairly well in accounting for odorant response phenomenology, there are still areas of active development. For example, there are heterogeneities across glomeruli in how effective normalization is at altering odorant responses (E. Hong, R.I.

Wilson, unpublished observations). Another open question is the functional significance of lateral excitation[19].

Information processing in the olfactory bulb in vertebrates reveals a more complex picture relative to *Drosophila*. Secondary neurons in vertebrates, called Mitral/Tufted cells (MT cells) send primary apical dendrites into a single glomerulus[20]. Like in *Drosophila,* the identity of the home glomerulus is an important determinant of the odorant selectivity of MT cells[21,22]. However, MT cells also possess basal dendrites which span a much larger area[20]. In accordance with the anatomy, functional interactions between glomeruli spanning large distances have been observed[23]. Interestingly, these interactions were found have a selective component: a "global" model that incorporates signals from a large area determined by the radius of basal projections performs poorly in describing MT cell responses, compared to a "sparse" model that allows strong excitatory and inhibitory influences from a small number of physically scattered glomeruli[23]. In addition to these selective influences, there is also evidence for a network of broad and diffuse signaling that can switch between having an excitatory or inhibitory effect depending on stimulus strength[24]. Furthermore, differences in response properties exist even between "sister" MT cells innervating the same glomerulus[22,25]. This is unlike the uniformity found in *Drosophila*[15].

In addition to having odorant selectivity in the magnitude of responses they produce, MT cells also use the timing of their responses as a coding variable[26,27]. Downstream areas are sensitive to the relative timing of activity in different glomeruli[28], and mice display behavioral sensitivity to the timing of MT cell responses relative to the breathing cycle[29]. Furthermore the two anatomical subtypes of MT cells, Mitral cells and

Tufted cells, have distinct and dynamic phase relationships relative to the breathing cycle of the animal[30]. Use of such temporal codes has been observed in locusts as well[31]. While this issue is not completely settled, to a first approximation *Drosophila* PNs do not appear to use fast temporal modulations of firing to encode odorant identity. Instead of generating diverse temporal patterns not directly related to stimulus dynamics like in vertebrates and locusts, *Drosophila* PNs appear to track odorant receptor neuron activity faithfully (K.I. Nagel, R.I. Wilson, unpublished observations).

These comparisons illustrate that the general organization of the olfactory system is conserved across vertebrate systems and *Drosophila*, but some important details are different. The early olfactory system of the fruitfly appears numerically smaller and operationally simpler. In both systems odorants are represented by multi-glomerular activity patterns and activity among glomeruli is interdependent. However in *Drosophila* activity patterns and interdependencies among glomeruli are more compactly describable, and the number of elements we must account for is much lower.

1.2 Higher-order olfactory processing: piriform cortex and the mushroom body

Multiple regions of the brain receive direct input from olfactory glomeruli. In these third-order regions, information coming from distinct channels is integrated and transformed, to produce novel representations of the olfactory world. Our understanding of this process is very preliminary. Only recently have we been getting glimpses at the answers to questions such as: how many glomeruli are pooled together in a typical third order olfactory neuron? Are there any rules that determine which glomeruli are integrated and which are not? Are signals from different glomeruli combined or compared? What

features of olfactory stimuli are represented through these operations? It is likely that different regions that receive glomerular inputs follow different rules of integration and will produce different answers to these questions. I will briefly discuss some of our current knowledge of higher olfactory areas in vertebrates and insects and then move on to discussing the specific area that will be the focus of the research presented in this dissertation.

It has been proposed as a basic principle that higher olfactory regions are functionally specialized such that they fall into two broad categories: those that perform primarily associative computations and underlie olfactory learning capabilities, and those that perform stereotyped computations and mediate innate olfactory behaviors[32–34]. While this theory may in the end not be the best way to conceptualize functional specialization among higher olfactory areas, it is a useful tool currently.

The "associative" areas are represented in mammals by piriform cortex, and in insects by the mushroom body. Neurons in both areas are generally very selective for odorants (i.e. they have high "lifetime sparseness"). From the population perspective, few neurons out of the whole population respond to any given odorant (i.e. there is high "population sparseness" in the representation of most odors)[35–40]. This is thought to be a useful strategy for a structure that is specialized for distinguishing potentially similar stimuli and associating them with reward information.

In both areas it appears that individual neurons receive inputs from multiple glomeruli [36,41,42] and they require the co-activation of at least a sizeable fraction of their inputs in order to produce an output[43,44]. In addition, lateral connections within both piriform cortex and the mushroom body strongly influence whether a given neuron

responds to an odorant[45–47]. On the whole, recruitment of odor responses tends to proceed non-linearly. Connectivity of glomerular inputs to third order neurons has been explored in more detail in the insect, where it appears that projections from glomeruli into the mushroom body have slight regional biases[48] and projections from similarly tuned glomeruli tend to wire together[43]. Overall, connectivity appears probabilistic[42] and the patterns of connectivity appear to be different in different individuals[49].

1.3 Higher-order olfactory processing: the lateral horn

In comparison to the piriform cortex and the mushroom body, the other, putatively "stereotyped" higher-order olfactory brain regions have received less attention. Among them are the mammalian cortical amygdala, the olfactory tubercle and the *Drosophila* lateral horn[32–34]. The lateral horn will be the focus of our investigations. The most famous functional result regarding the lateral horn, and one of the reasons for the production of the "associative vs. stereotyped" theory, is the observation that ablating the mushroom body impairs the ability of flies to perform olfactory association tasks, but spares their unlearned preferences for odorants[50,51]. Since the lateral horn is the only higher olfactory area left intact when the mushroom body is ablated, this observation led to the idea the lateral horn must mediate innate odor driven behaviors[52].

Anatomical evidence agrees with the notion that the lateral horn mediates operations that do not vary from animal to animal. Across individual animals, individual olfactory glomeruli project with bias to highly stereotyped subregions of the lateral horn[53]. This is also the case for the cortical amygdala[32,33]. Such biases are of lesser degree in the projections to the mushroom body[48]. It has been unclear however, to what extent

stereotypy in projection patterns translates to cellular connectivity. It is important to note that the number of projections into these areas also differs. While the lateral horn contains many fewer neurons than the mushroom body, it actually receives a larger proportion of the output of the Antennal Lobe. This difference is mainly due to the previously mentioned smaller cluster of multiglomerular GABAergic neurons that project out of the Antennal Lobe[9,10,54]. These neurons bypass the mushroom body and target only the lateral horn.

We know little about how neurons in the lateral horn (or the olfactory tubercle or the cortical amygdala) integrate their inputs, and how they represent odorants. A recent study revealed that the lateral horn contains a cluster of neurons that receives input from a single glomerulus, and which is devoted to the processing of pheromones[55]. This raises the possibility that signals from different glomeruli remain segregated in the lateral horn. On the other extreme, a recent study in locusts found that lateral horn neurons were very broadly tuned to odors, and suggested that these neurons receive massively convergent glomerular inputs[56]. A theoretical study proposed a plausible third alternative: that lateral horn neurons (LHNs) might add and subtract sparse, weighted inputs from coactivated glomeruli[34]. This latter study also suggested that some combinations of glomeruli should be overrepresented, namely, glomeruli whose sum or difference represents a behaviorally useful computation. Overall, it is unclear which of these scenarios best describes lateral horn neurons.

1.4 Summary of our approach

Our ultimate goal is to understand what a higher order olfactory receptive field

looks like. Unfortunately the notion of "receptive field" is most useful and satisfying when the stimulus feature detected by the receptive field is intuitive for us. Whereas the notion of "visual features" is intuitive (e.g., edges, contours, objects), an "olfactory feature" is a nebulous concept. This would not be an issue if we could construct odor sets based on a principled approach to the statistics of natural odorants. However olfactory stimulus space is high dimensional, natural olfactory stimuli are complex, and our understanding of the natural statistics of odorants is relatively poor. This makes constructing a biased but principled or un-biased stimulus set difficult. Even with very large odor sets, it is difficult to link the selectivity of a neuron for particular monomolecular odorants to an intuitively appealing "olfactory feature" that might be behaviorally useful to the animal. The only context in which this is easier is in the case of very special stimuli like pheromones. A promising approach in identifying salient non-pheromonal stimuli is found in studies that combine delivery of particular natural stimuli with simultaneous gas chromatography and neural recording.[57]

The ability to target identified neurons and the numerical simplicity of the fruit fly olfactory system offers an alternative way to describe the stimulus selectivity of higher olfactory neurons in intuitive terms. We reasoned that if the lateral horn contains stereotyped neurons that are physiologically invariant across animals, we should be able to target them with selective genetic labels and determine, for individual lateral horn neurons,

- their odorant selectivity
- their feedforward inputs
- the odorant selectivity of their inputs

- how they integrate their inputs

Ultimately we aim to construct a picture of how sensory information is reformatted as it travels through identified connections into a higher order olfactory area. The majority of this dissertation documents the results of this effort.

In chapter 4, I describe new techniques we have been developing in order to map feedforward connectivity in a higher throughput manner. This is a natural continuation of our previous work, because in our initial study we were only able to describe the form of transformations (with limitations) for what is essentially just two lateral horn neuron subtypes – a small fraction of the ~100 subtypes that likely exist in the lateral horn. Ideally we would like to assemble a description of how populations of third order neurons sample from the glomerular array. We would like to determine the functional relationships that dictate which glomeruli are integrated, combined or compared. Only then can we relate "patterns" of connectivity with particular "patterns" of stimulus selectivity and thereby get a picture of how these higher olfactory neurons divide up olfactory stimulus space and extract useful information. This work is currently ongoing and promising, but has not produced any biological insight yet.

Chapter 2

General Methods

2.1 Fly stocks

Flies were raised in intermediate-density cultures on conventional cornmeal agar medium supplemented with rehydrated potato flakes (Carolina Biological Supply) under a 12 h light, 12 h dark cycle at 25 °C. All experiments were performed on adult female flies within the first 2 days after eclosion. The genotypes used, by figure, are listed in table below.

Table 1. Transgenic fly lines used by figure

Figure 1a	*UAS-C3PA-GFP;UAS-SPA-GFP/nsyb-Gal4*
Figure 1b	*pJFRC7-20XUAS-IVS-mCD8::GFP(attp40)/+;GMR73B12-Gal4/+*
Figure 1c	*pJFRC7-20XUAS-IVS-mCD8::GFP(attp40)/+; GMR44G08-Gal4/+*
Figure 1d	*Mz671-Gal4,UAS-CD8:GFP*
Figure 1e	*NP6099-Gal4,UAS-CD8:GFP*
Figure 2a	*pJFRC7-20XUAS-IVS-mCD8::GFP(attp40)/+;GMR48F03-Gal4/+* and *pJFRC7-20XUAS-IVS-mCD8::GFP(attp40)/+;GMR73B12-Gal4/+*
Figure 2b	*pJFRC7-20XUAS-IVS-mCD8::GFP(attp40)/+;GMR12H12-Gal4/+* and *pJFRC7-20XUAS-IVS-mCD8::GFP(attp40)/+; GMR44G08-Gal4/+*
Figure 2c,e	*Mz671-Gal4,UAS-CD8:GFP*
Figure 2d,f	*NP6099-Gal4,UAS-CD8:GFP*
Figure 3 LHN, DM1 PN pairs LHN, DM2 PN pairs LHN, DM4 PN pairs LHN, DL5 PN pairs LHN, DM6 PN pairs LHN, DC1 PN pairs	 *NP5221-Gal4,Mz671-Gal4;UAS-CD8:GFP* *Mz671-Gal4,UAS-CD8:GFP;c3l5-Gal4,UAS-CD8:GFP* and *GH146-Gal4,UAS-CD8GFP/Mz671-Gal4,UAS-CD8:GFP* and *NP5221-Gal4,UAS-CD8:GFP/Mz671-Gal4,UAS-CD8:GFP* *NP3062-Gal4,UAS-CD8:GFP;Mz671-Gal4,UAS-CD8:GFP* *NP3062-Gal4,UAS-CD8:GFP;Mz671-Gal4,UAS-CD8:GFP* *NP3062-Gal4,UAS-CD8:GFP;Mz671-Gal4,UAS-CD8:GFP* *Mz671-Gal4,UAS-CD8:GFP;c3l5-Gal4,UAS-CD8:GFP*
Figure 4 LHN, DM1 PN, DM2 PN triplets LHN, DM1 PN, DM4 PN triplets	 *NP5221-Gal4,Mz671-Gal4;c3l5-Gal4,UAS-CD8:GFP* *NP3062-Gal4,UAS-CD8:GFP;NP5221-Gal4,Mz671-Gal4*
Figure 5 Lateral Horn Neurons DM1 PNs DM4 PNs	 *Mz671-Gal4,UAS-CD8:GFP* *NP5221-Gal4,UAS-CD8:GFP* *NP3062-Gal4,UAS-CD8:GFP;*
Figure 6	Same as figure 4 and 5 above

Table 1 (continued): Transgenic fly lines used by figure

Figure 7	*NP6099-Gal4;GH146-Gal4/UAS-C3PA-GFP;UAS-SPA-GFP/+*
Figure 8a,b LHNs DP1m PNs LHN DP1m pairs (blue points)	 *NP6099-Gal4,UAS-CD8:GFP* *GH146-Gal4/UAS-C3PA-GFP;UAS-SPA-GFP/+* *NP6099-Gal4/+;GH146-Gal4/UAS-C3PA-GFP;UAS-SPA-GFP/+*
Figure 8c Wild type LHNs *Orco*^{2} LHNs *IR64*^{MB05283} LHNs	 *NP6099-Gal4,UAS-CD8:GFP* *NP6099-Gal4,UAS-CD8:GFP;+/+;Orco*^{2} *NP6099-Gal4,UAS-CD8:GFP;+/+;Ir64a*^{MB05283}
Figure 9	Same as Figure 8a
Figure 10 LHNs in intact preparations LHNs with transection of iPN and/or ePN axons	 *NP6099-Gal4,UAS-CD8:GFP* *NP6099-Gal4,UAS-CD8:GFP/+;GH146-Gal4,UAS-CD8:GFP/+*
Figure 11 Type I and II LHNs Lateral horn local neurons	 same as Figure 2 *pJFRC7-20XUAS-IVS-mCD8::GFP(attp40)/+;GMR23F06-Gal4/+*
Figure 12 A B	 *NP6099-Gal4,UAS-CD8:GFP* *pJFRC7-20XUAS-IVS-mCD8::GFP(attp40)/+;GMR73B12-Gal4/+* *pJFRC7-20XUAS-IVS-mCD8::GFP(attp40)/+;GMR48F03-Gal4/+*
Figure 14	*pebbled-Gal4/+; UAS-CD8:GFP/+: UAS-P2X*$_2$
Figure 15	*pebbled-Gal4/+; UAS-CD8:GFP/+: UAS-P2X*$_2$

In addition to the glomeruli listed above in the corresponding section, we also targeted additional glomeruli for paired recordings from PNs and *Mz671* neurons, as noted in the text; these were the following glomeruli, with the Gal4 lines used to target them in parentheses: VA4 / VC1 / VC2 (*NP5221-Gal4*), VL2a (*NP3062-Gal4*), VM2 (*NP3481-Gal4* and *NP3062-Gal4*), VM7 (*GH146-Gal4*). *NP6099-Gal4* was obtained from the Drosophila Genetic Resource Center (DGRC) at the Kyoto Institute of Technology. The following stocks were obtained from the Bloomington Stock Center: *Ir64a*^{MB05283} (#24610), *nsyb-Gal4 (*#39171*), GMR48F03-Gal4* (#50373, type I LHNs), *GMR73B12-Gal4* (#39814, type I LHNs), *GMR12H12-Gal4* (#48534, type II LHNs), *GMR44G08-Gal4* (#50216, type II LHNs), *GMR23F06-Gal4* (#49036, lateral horn local

neurons). Genotypes were previously published as follows: *Mz671-Gal4*, *NP6099-Gal4*, and *NP5221-Gal4*[48]; *pebbled-Gal4*[58]*, nsyb-Gal4* (also known as *GMR57C10-Gal4*) and all other *GMR* lines[59] ;*UAS-C3PA-GFP* and *UAS-SPA-GFP* (these transgenes express different variants of PA-GFP under UAS control[55]; *UAS-CD8:GFP*[60] ; *c315a-Gal4*[61]*; GH146-Gal4*[62]*; NP3062-Gal4*[63]; *NP3481-Gal4*[17]; *Orco*[2] (ref[64]); *Ir64a*[MB05283] (ref[65]). *pJFRC7-20XUAS-IVS-mCD8::GFP(attp40)* is described in Tuthill, et. al[66] and was initially published in another insertion site (attP2)[59]. The GMR lines used here that have not been previously published are as follows: *GMR48F03-Gal4* (type I LHNs) labels ~10 neurons; *GMR73B12-Gal4* (type I LHNs) labels ~10 neurons; *GMR12H12-Gal4* (type II LHNs) labels ~20 neurons; *GMR44G08-Gal4* (type II LHNs) labels ~20 neurons; *GMR23F06-Gal4* (lateral horn local neurons) labels ~25 neurons. These numbers were obtained by visually inspecting confocal images publicly available at http://flweb.janelia.org[59].

2.2 Electrophysiology

In vivo whole cell patch clamp recordings were performed as previously described[60]. Generally one neuron was recorded per brain. The internal patch pipette solution contained (in mM): potassium aspartate 140, HEPES 10, MgATP 4, Na_3GTP 0.5, EGTA 1, KCl 1, biocytin hydrazide 13 (pH = 7.3, osmolarity adjusted to ~ 268 mOsm). The external saline contained (in mM): NaCl 103, KCl 3, N-tris(hydroxymethyl) methyl-2-aminoethane-sulfonic acid 5, trehalose 8, glucose 10, $NaHCO_3$ 26, NaH_2PO_4 1, $CaCl_2$ 1.5, and $MgCl_2$ 4. Osmolarity was adjusted to 270–273 mOsm. The saline was bubbled with 95% O_2/5% CO_2 and reached a final pH = 7.3. Recordings were obtained

with an Axopatch 200B model amplifier with a CV-203BU headstage and acquired with custom written IgorPro or Matlab routines. Recorded voltages and currents were low-pass filtered at 5 kHz prior to digitization at 10 kHz. Patch pipettes were made from borosilicate glass (Sutter, 1.5 mm o.d., 0.86 mm i.d.) and were fire polished using a microforge (Narishige). For some lateral horn neuron recordings, the patch pipette was pressure-polished to reduce resistance as described previously[41]. The estimated final pipette tip opening was submicron in diameter, with pipette resistance between 10-15 MΩ. In "randomly-targeted" PN recordings, PNs were not labeled with a visible marker, but were identified based on their cell body location and characteristic intrinsic properties. In these "randomly-targeted" PN recordings, we made an effort to sample PN somata in both the anterodorsal cluster and the lateral cluster, and also to sample both large and small somata, but these recordings are nonetheless probably somewhat biased toward large somata in the anterodorsal cluster. In some experiments we removed one or both antennae to allow for easier access to the antennal lobe. Recordings from DP1m PNs and VA2 PNs were performed using PA-GFP to target our recording electrode to the PN soma (see below). For the paired recording experiments from *NP6099* LHNs and DP1m PNs or VA2 PNs, in order to gain the necessary optical and mechanical access to the antennal lobe and lateral horn, we removed the brain from the head capsule and pinned it in a Sylgard-coated dish.

2.3 Odor delivery

An air stream (2.005 L/min) was passed through activated carbon and directed at the fly through a carrier tube (6.3 mm inner diameter) and positioned 15 mm from the fly.

The fly was positioned to face away from the carrier tube. 5 mL/min of this air stream (the "odor stream") was diverted from the carrier and directed by a 3-way solenoid valve into the headspace of a clean 1-mL vial (National Scientific, C4011-5W) containing 200 μL of a solution of odor in paraffin oil, or else an identical empty vial. The solenoid normally directed the odor stream to the empty vial, and switched airflow into the odor vial upon receiving a command. After passing through either vial the odor stream joined the carrier stream again. Odor dilutions refer to the dilution factor by volume of odor in solvent. Odor pulses were 500 ms in duration with an inter-pulse interval of 40 sec. Because the odor stream flow rate is relatively low, we reduced the distance the stream has to travel from the solenoid to the vials (9 cm) and the from the vials back into the carrier stream (1 cm). Odor dilutions in paraffin oil were prepared fresh daily, and vials were used for only one experiment before they were discarded. Paraffin oil was stripped of low molecular weight volatiles by storing under negative pressure, generally for at least several days prior to use. Based on previous work, we know that methyl acetate is relatively selective for DM4 olfactory receptor neurons at low concentrations[18], which is relevant to the design of experiments where we deliver concentration series of this odorant. This previous study used a slightly different olfactometer, but in calibration experiments, we verified that the olfactometer we used in this study delivered if anything somewhat more dilute stimuli than those delivered by the previous study at the same nominal dilution.

2.4 Two-photon laser scanning microscopy, photoactivation and laser transection

Photoactivation of PA-GFP[67,68] was performed for anatomical investigation in the lateral horn and to target PNs for whole cell recordings in cases where no specific Gal4 line was available. We used a custom built 2-photon laser scanning microscope running ScanImage acquisition software[69]. For both anatomy and targeting, we used a procedure similar to that described previously[55,68]. Briefly, the neuropils of interest were identified using the resting fluorescence of PA-GFP at the imaging wavelength (925 nm). After defining volumes of interest based on these background images, PA-GFP was photo-converted by imaging through the volume with 710 nm light. In each photoactivation block, we moved through the z-depth of the volume of interest with 0.25 μm steps, imaging each z-frame 3 times. We adjusted laser power on an experiment-by-experiment basis. After PA-GFP is photoactivated in the neuropil (i.e., axons and dendrites), it diffuses into the somata of the corresponding neurons.

In anatomical experiments where we sought to explore the morphology of all lateral horn neurons without targeting subtypes, we photoactivated in a large portion of the dorsal lateral horn, taking care not to directly photoactivate any cell bodies. We performed three photoactivation blocks separated by 5 minute inter-block intervals. Based on several such experiments, we conservatively estimate that there are at least one dozen type I and two dozen type II neurons on each side of the brain.

For the physiology experiments where we targeted particular PNs with PAGFP, we located the desired glomerulus and photoactivated in a volume of several μm^3 that was entirely circumscribed by that glomerulus. In order to confirm that the recorded PN did indeed arborize in the correct glomerulus, we filled every recorded PN with biocytin, visualized it using a fluorescent streptavidin conjugate, and inspected it *post hoc*, using

nc82 antibody to label glomerular compartments (see below). In these experiments, we performed only one photoactivation block (rather than three) in order to avoid damaging brain tissue before the recording.

For laser transection experiments, we labeled the inner antenno-cerebral tract (iACT) and middle antenno-cerebral tract (mACT) by expressing GFP under the control of *GH146-Gal4*. The iACT contains the axons of excitatory PNs, and the mACT contains the axons of inhibitory PNs. The iACT was transected between the mushroom body calyx and the lateral horn. The mACT was transected where it appears from beneath the mushroom body peduncle before it enters the lateral horn. For both transection experiments we defined volumes of interest that completely circumscribed the tract we aimed to cut. Volumes were approximately 5-10 μm on each side. In order to transect the tract, we scanned through the depth of these volumes once or twice in 0.5-μm steps for approximately 0.5 s dwell time per frame. Laser power at the back aperture of the objective was 50-80 mW at 800 nm, the transection wavelength. The volume, imaging duration, and laser power was adjusted on an experiment-by-experiment basis so as to achieve a visible cavitation bubble that encompassed the axon tract.

2.5 Immunohistochemistry and anatomy

In order to ascertain or confirm the glomerular identity of recorded PNs, we filled them with biocytin and visualized the fills with fluorescent conjugated streptavidin. This was done in two situations. First, every time we recorded from a GFP-labeled PN, we filled it to confirm its putative identity. Second, in random recordings from unlabeled PNs, we filled PNs that turned out to be connected to simultaneously-recorded LHNs. To

identify glomeruli, the glomerular neuropil was visualized using fluorescence immunohistochemistry with nc82 antibody (Developmental Studies Hybridoma Bank, nc82-s, 1:50 dilution).

In some experiments, the identity of the recorded LHNs was confirmed in a similar manner. The morphology of single dye-filled LHNs was compared with an atlas of brain neuropil divisions (www.virtualflybrain.org) in order to determine the region(s) where LHN axons arborized. Type I neurons arborized in the superior medial protocerebrum, as noted previously[48], but its arbors also extend into the superior intermediate protocerebrum and the crepine. Type II neurons arborized in the superior lateral protocerebrum, as noted previously[48].

The protocol for processing these fills has been described previously[14]. To reconstruct neuronal morphology from biocytin fills, we hand-traced the skeletonized morphology using the Simple Neurite Tracer plugin in Fiji (http://fiji.sc), using the Fill Out command to automatically generate a 3D volume, which we subsequently converted to a *z*-projection. Triple immunofluorescence against GABA (Sigma A2052), CD8, and nc82 was performed essentially as previously described[60] except that a different anti-CD8 antibody was used (Invitrogen MCD0800, 1:50) and the anti-nc82 antibody was used at a dilution of 1:50.

2.6 Analysis

2.6.1 Spike detection

Spikes were detected using custom written Matlab routines. A two-threshold routine was used to detect the events in the voltage trace that were both the fastest to rise

and also the fastest to decay. The first threshold was initially used to detect positive peaks in the second time derivative of the voltage trace in order to pick out the fastest rising events. Next, a threshold was used to detect negative peaks in the first time derivative of the voltage trace in the time window [–0.3 ms,+12 ms] around the second derivative threshold crossing. Both thresholds were set manually and independently for each recording, in order to accurately capture the spikes identified by visual inspection. Automated spike detection with this routine was robust at spontaneous and lower odor-evoked firing rates. However at the higher firing rates produced by type I LHNs, action potential size became very small and post hoc visual inspection became necessary to correct errors. In order to ensure that our results in concentration series experiments were not affected by experimenter intervention in spike detection, we blinded the spike detector to the stimulus concentration. In roughly a quarter of the cells we recorded from in our recordings of odor responses, spike sorting could not be performed reliably. Those recordings were excluded from analysis.

2.6.2 Odor response metrics

In cases where we measure odor-evoked spike counts, we counted spikes over a 1-s window starting at the odor onset command. The odor valve remained open for 500 ms. Due to the construction of our olfactometer, there was a ~150-ms delay from when the odor onset command is sent by the acquisition computer to the solenoid to the time odorant reaches the fly, as determined using a fast photoionization detector at the fly's location (mini-PID, Aurora Scientific). As both LHN types showed relatively low levels of spontaneous spiking, we simply counted spikes over a 1 sec window starting at the

odor onset command, in order to ensure that all odor-evoked spiking was captured. Lifetime sparseness of odor-evoked spike count data was computed as described previously[35], except that the baseline firing rate (which was always close to zero) was not subtracted from odor-evoked firing rates.

2.6.3 Spike-triggered averages of postsynaptic voltage

The existence of a monosynaptic connection between a projection neuron and the lateral horn neuron was assessed using spike-triggered averaging of the lateral horn neuron membrane potential, triggered on single PN spikes. On each trial, we injected a brief (30-100 ms) step of depolarizing current into the PN via the patch pipette to elicit a single action potential. We obtained between 16 and 250 trials for each paired recording. We aligned the postsynaptic voltage trace to the time of the peak of the presynaptic action potential, defined as time t=0. We averaged over the time window t=-20 ms to t=80 ms and defined the average voltage in the window -20 ms to 0 ms as the baseline. An EPSP was said to occur if in the time window t=0 ms to t=5 ms the spike-triggered average crossed a threshold of +5 standard deviations computed over the 20 ms baseline period. In most experiments we triggered only single action potentials in PNs, but in 4 experiments we also included data from trials where up to three PN spikes were evoked (using a 100-ms step of current injection in the PN). This could potentially bias EPSP amplitudes; however these four experiments revealed no connection. EPSP amplitude was measured as the baseline-subtracted peak depolarization in the time window t=0 to t=20 ms. EPSP latency was defined as the time of extrapolated zero-crossing of linear fits to the 20-80% rising phase of the spike-triggered average.

2.6.4 Triplet recordings

In order to determine subthreshold contributions on individual PNs, we measured changes in LHN membrane potential (V_m) while presynaptic PNs were stimulated with a 500-ms step of depolarizing current. For this measurement, V_m was first low-pass filtered to remove spikes. We then computed average V_m over a steady-state period during the stimulus (100 – 500 ms after stimulus onset) and we subtracted the average V_m over a baseline period preceding the stimulus.

2.7 Modeling

In order to model contributions of individual PNs to the spiking output of LHNs, we fit LHN spike counts with the following equations:

$$LHN_{PN1} = R_{max1}\frac{1}{1+\sigma_1{}^{n_1}/(PN_1)^{n_1}}$$

$$LHN_{PN2} = R_{max2}\frac{1}{1+\sigma_2{}^{n_2}/(PN_2)^{n_2}}$$

where PN_1 and PN_2 are spike counts associated with the first and second PNs, respectively. LHN_{PN1} and LHN_{PN2} are spike counts of the LHN on trials where only one PN was active. The equations define input-specific sigmoid nonlinearities, where the fitted parameters [R_{max1}, R_{max2}] are the amplitudes of the sigmoids and can be interpreted as the weights associated with the two inputs. The fitted parameter σ is the semi-saturation constant (i.e., the level of PN input at which the LHN response is half-maximal). The fitted exponential parameter n represents the shape and steepness of the sigmoid.

In order to model the integration of individual inputs by LHNs, we fit the 3-dimensional transformation from presynaptic spike counts to postsynaptic spike counts with the surface defined by the following equation:

$$LHN_{total} = LHN_{PN1} + LHN_{PN2}$$

where the parameters were fixed at the values obtained above from fitting the transformation for individual PN inputs. In other words, we predicted the postsynaptic spiking response to combined activation of two inputs simply as the sum of the responses to each input alone. This model yielded a reasonable prediction of the actual spike counts obtained (R^2=0.69). Much of the residual variance represents measurement uncertainty (i.e., trial-to-trial or cell-to-cell variation), and so cannot be accounted for by any model of this kind.

We also fit the same data set with an alternative model that incorporates a third term:

$$LHN_{total} = LHN_{PN1} + LHN_{PN2} + C(LHN_{PN1} * LHN_{PN2})$$

where the third term represents a multiplicative interaction between the two PN inputs, and *C* is the coefficient of the interaction term. Again the parameters for LHN_{PN1} and LHN_{PN2} were fixed at the values obtained from fits to individual PN input transformations. This model did not improve fit quality (R^2 = 0.69). Furthermore, the fitted coefficient *C* of the interaction term was two orders of magnitude smaller than R_{max1} and R_{max2}. In other words, there was a minimal contribution from the multiplicative term. This indicates the data is adequately explained as a sum over PN inputs, and

including a cooperative interaction between the two PN inputs provides no additional explanatory power.

Chapter 3

Transformation of olfactory information in lateral horn neurons

3.1 Two morphological types of lateral horn neurons

To visualize all lateral horn neurons, we expressed photoactivatable GFP (PA-GFP) pan-neuronally and used 2-photon excitation microscopy to activate GFP throughout the lateral horn neuropil, so that activated PA-GFP labels most neurons that have neurites in the lateral horn. We observed several large clusters of labeled somata. One cluster was dorsomedial to the lateral horn neuropil, and one cluster was ventrolateral (Figure 1a). Both clusters are connected to major neurite tracts that enter and exit the horn at distinctive locations. We define these as type I and type II neurons, respectively. Together, these clusters comprise a substantial fraction of all labeled somata, although they do not encompass all morphological types[48].

Through a visual screen of ~7000 Gal4 enhancer trap lines[59] we obtained two lines that label a large fraction of type I neurons, along with two lines that label a large fraction of type II neurons. We used these lines to drive GFP expression and we biocytin-filled a sample of GFP+ neurons using *in vivo* whole-cell patch clamp recordings. These fills revealed that type I neurons all innervate the superior medial protocerebrum, although they differ in their fine morphological structure. The same was true of type II neurons and the superior lateral protocerebrum (Figure 1b,c; see also Chapter 2).

Figure 1. Two morphological types of lateral horn projection neurons.

A. Z-projection of a coronal 2-photon stack through a portion of the brain. PA-GFP is expressed pan-neuronally (under the control of *n-synaptobrevin-Gal4*) and photo-converted throughout the lateral horn (LH) neuropil. Magenta circle marks the boundary of the lateral horn. Arrows mark the three clusters of somata described in this study: type I, type II, and lateral horn local neurons (LNs; see below). The antennal lobe (AL) is weakly labeled because PN axons are photoconverted. Dorsal is up, lateral is right. Similar results were obtained in a total of 4 experiments.

B-C. Morphologies traced from biocytin-filled single neurons, where recorded neurons expressed GFP under the control of the indicated Gal4 lines. Somata were detached when the pipette was removed and so are symbolized by gray circles. Type I neurons have dendrites in the lateral horn and project to the superior medial protocerebrum (SMPC). Type II neurons have dendrites in the lateral horn and project to the superior lateral protocerebrum (SLPC). Two examples are shown for each type. Morphologies similar to the examples shown here were observed in all neurons of a given type (n = 8 for each). In type I fills we noted minor variations across cells, including a small projection to the mushroom body (MB) calyx in two cases.

D-E. The morphologies of *Mz671* neurons (type I subtype) and *NP6099* neurons (type II subtype) were all essentially identical to the examples shown here (n=7 and 10).

Figure 1 (continued): Two morphological types of lateral horn projection neurons.

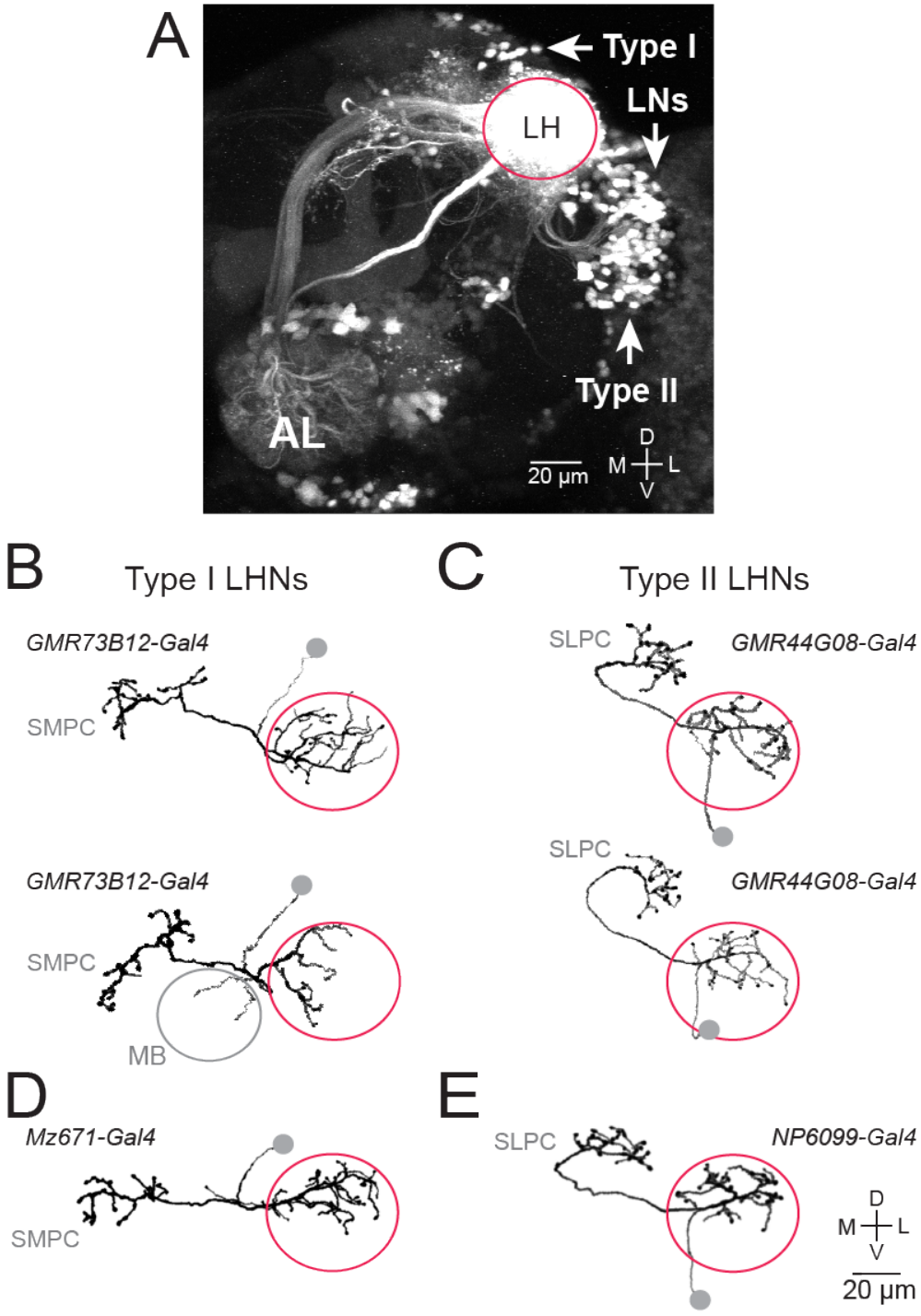

Two enhancer trap lines have been identified previously which label small numbers of neurons having these morphologies. Specifically, *Mz671-Gal4* labels three type I neurons on each side of the brain, and *NP6099-Gal4* labels three type II neurons[48,53]. We used single-cell biocytin fills to confirm these morphologies (Figure 1d,e). These lines provide genetic access to small, genetically-defined subsets of neurons belonging to each major type.

3.2 Odorant selectivity in type I and type II lateral horn neurons

We next surveyed the odor responses of the type I and type II populations, using the Gal4 lines that drive expression in large numbers of neurons within each type to label these neurons with GFP. We made *in vivo* whole-cell patch clamp recordings from a sample of GFP+ neurons within each line. We used a test panel of chemically diverse odors in these experiments in order to coarsely sample odor space. Because these Gal4 lines label many cells, we expect the labeled cells to exhibit diverse odor preferences. Indeed, within each morphological type, we found that different neurons had different preferred odors (Figure 2a,b). Interestingly, we found a systematic and significant difference between the odor tuning of type I and type II neurons: the former were broadly tuned, whereas the latter were more selective.

We then focused specifically on the small numbers of type I and type II neurons defined by *Mz671-Gal4* and *NP6099-Gal4*. We found that all three of the *Mz671* neurons showed stereotyped odor responses, both within brains and across brains. Like most type I neurons, they were broadly tuned (Figure 2c).

Figure 2. Odor selectivity in type I and type II neurons.

A. Odor selectivity of a population of type I neurons. Spikes are counted over a duration of 1 s starting at the odor onset command. Each data point is the trial-averaged response to one odor in one experiment, with a line connecting all the responses from the same experiment (n=4 from *GMR48F03-Gal4* [solid] and 4 from *GMR73B12-Gal4* [dashed]). All odors are 10^{-2} dilutions in paraffin oil (solvent), except where noted. Note the relatively broad tuning of type I neurons.

B. Same for a population of type II neurons (n=4 from *GMR44G08-Gal4* [solid] and 4 from *GMR12H12-Gal4* [dashed]; note that some neurons did not spike in response to any odor, but all showed subthreshold responses). Tuning is significantly narrower in type II neurons as compared to type I neurons (unpaired two-tailed t-test comparing lifetime sparseness [see Methods], P=0.0014, d.f. = 14).

C. Within a subtype of type I neurons (labeled by *Mz671-Gal4*), odor selectivity is stereotyped (n=6). The trace shows a typical *in vivo* whole-cell current clamp recording from one of these neurons. In all figures, a thick horizontal line indicates the 500-ms period when the odor valve was open.

D. Same as panel c but for the subtype of type II neurons labeled by *NP6099-Gal4* (n=8). The trace shows a typical recording from one of these neurons. Tuning is significantly narrower in *NP6099* neurons as compared to *Mz671* neurons (unpaired two-tailed t-test, $P=1.9\times10^{-8}$, d.f.=12).

E. Responses to an odor concentration series. Traces are averaged across trials and neurons (± s.e.m. across neurons). Responses are steady over time and grow monotonically with concentration.

F. Same as panel e for *NP6099* neurons (n=8). Responses are more transient and are suppressed at high concentrations, suggesting the recruitment of inhibition.

Figure 2 (continued): Odor selectivity in type I and type II neurons.

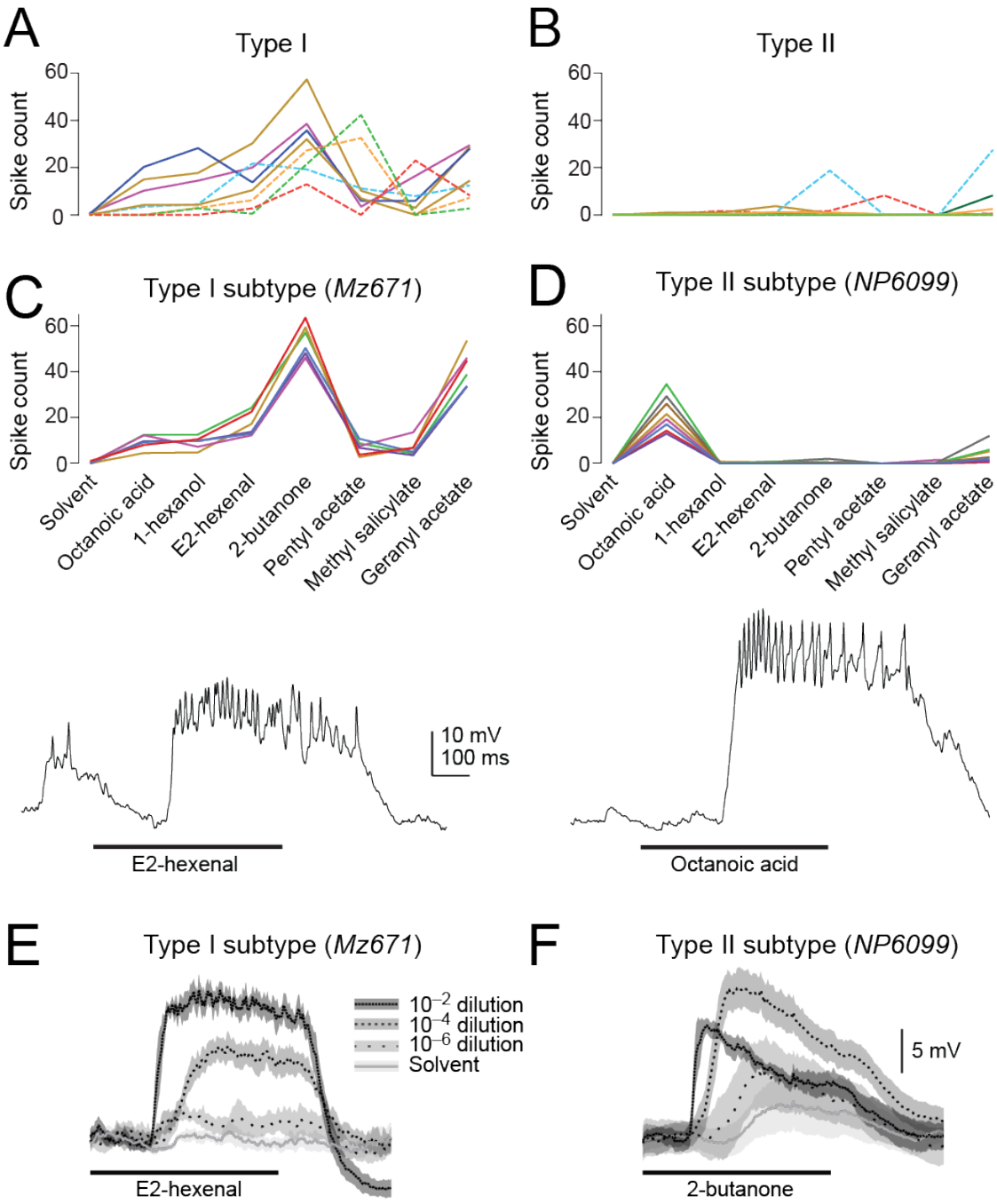

Similarly, *NP6099* neurons also showed stereotyped odor responses, both within and across brains. Like most type II neurons, they were narrowly tuned (Figure 2d). Thus, the morphologies of both *Mz671* neurons and *NP6099* neurons accurately predicted their tuning breadth.

In addition, we noticed differences in the concentration tuning of these neurons. The responses of *Mz671* neurons grew monotonically over a large dynamic range of concentrations. By contrast, the responses of *NP6099* neurons were suppressed by high concentrations, and also became more transient at high concentrations (Figure 2e,f). This suggests that some of the odor responses of *NP6099* neurons might be suppressed by inhibition.

In sum, these results show that type I and type II neurons differ systematically in the breadth of their odor tuning. The *Mz671* neurons and the *NP6099* neurons are exemplars of each type. In order to understand the connectivity that underlies the odor responses of lateral horn neurons of each type, we focus in the rest of this study on the *Mz671* and *NP6099* neurons.

3.3 Connectivity from glomeruli onto type I neurons

We next screened for connections from antennal lobe projection neurons (PNs) onto lateral horn neurons, using paired *in vivo* whole cell patch clamp recordings, and focusing initially on the *Mz671* population. In every experiment we targeted one electrode to one *Mz671* neuron and one randomly-selected PN, depolarizing each PN with direct current injection so that it fired one spike per trial. In most cases the cells were not connected. In a small minority of pairs, we observed excitatory postsynaptic

potentials with short and consistent latencies (<1.5 ms), indicative of monosynaptic connections (Figure 3a). In these cases, we filled the PN with biocytin for *post hoc* identification.

In this screen, we performed 120 separate paired recordings and obtained five connected pairs. All the PNs in these pairs innervated one of three glomeruli (DM2, DM4, VA7l). This connection rate implies that the *Mz671* neurons receive input from only a handful of glomeruli – nominally four or fewer glomeruli if we were to assume unbiased sampling (see Discussion).

To ask whether connections are stereotyped, we performed paired recordings where antennal lobe PNs were labeled with GFP rather than randomly selected. We selectively targeted PNs in twelve glomeruli: two that emerged from our screen (DM2 and DM4), plus 10 others (DC1, DL5, DM1, DM6, VA4, VC1, VC2, VL2A, VM2, VM7). We did not have a genetic label for the VA7l glomerulus. All PNs recorded in this data set were filled with biocytin to confirm their identity.

These experiments showed that connectivity from PNs to *Mz671* neurons was invariant. Three glomeruli were always or almost always connected (DM1, DM2, DM4), and the other 10 glomeruli were never connected (Figure 3b and legend). Notably, a stereotyped synaptic weight was associated with each connected glomerulus: DM1 consistently evoked larger synaptic responses than either DM2 or DM4.

Figure 3. Paired recordings identify convergent glomerular inputs.

A. An example paired recording from a GFP+ *Mz671* neuron and one of its presynaptic PNs. Top trace is a single PN spike evoked by direct current injection. Bottom traces are postsynaptic membrane potentials in individual trials (thicker line is the trial-averaged response). Vertical scale for postsynaptic responses is the same as panel b.

B. Results from multiple experiments of this type. In these experiments, both the pre- and postsynaptic neuron were GFP+. A single row shows trial-averaged postsynaptic responses from five paired recordings, each in a different brain. Shown at left are z-projections of confocal stacks through the antennal lobe displaying the dendritic tufts of biocytin-filled PNs (scale bars 10 μm), together with the total number of connections observed and total number of pairs recorded. DM1 consistently evoked larger responses than either DM2 or DM4 (1-way ANOVA, $F(2,16)=12.45$, $P=5.5\times10^{-4}$, followed by *post hoc* unpaired two-tailed *t*-tests, DM1 vs. DM2: $P=0.015$, d.f.=12, DM1 vs. DM4: $P=0.019$, d.f.=8). Note that some responses have a transient peak (arrow) which likely reflects a contribution of voltage-gated postsynaptic conductances. Data are not shown for the following glomeruli, none of which were connected: VA4 (0/1), VC1 (0/3), VC2 (0/3), VL2A (0/1), VM2 (0/2), VM7 (0/2).

Figure 3 (continued): Paired recordings identify convergent glomerular inputs.

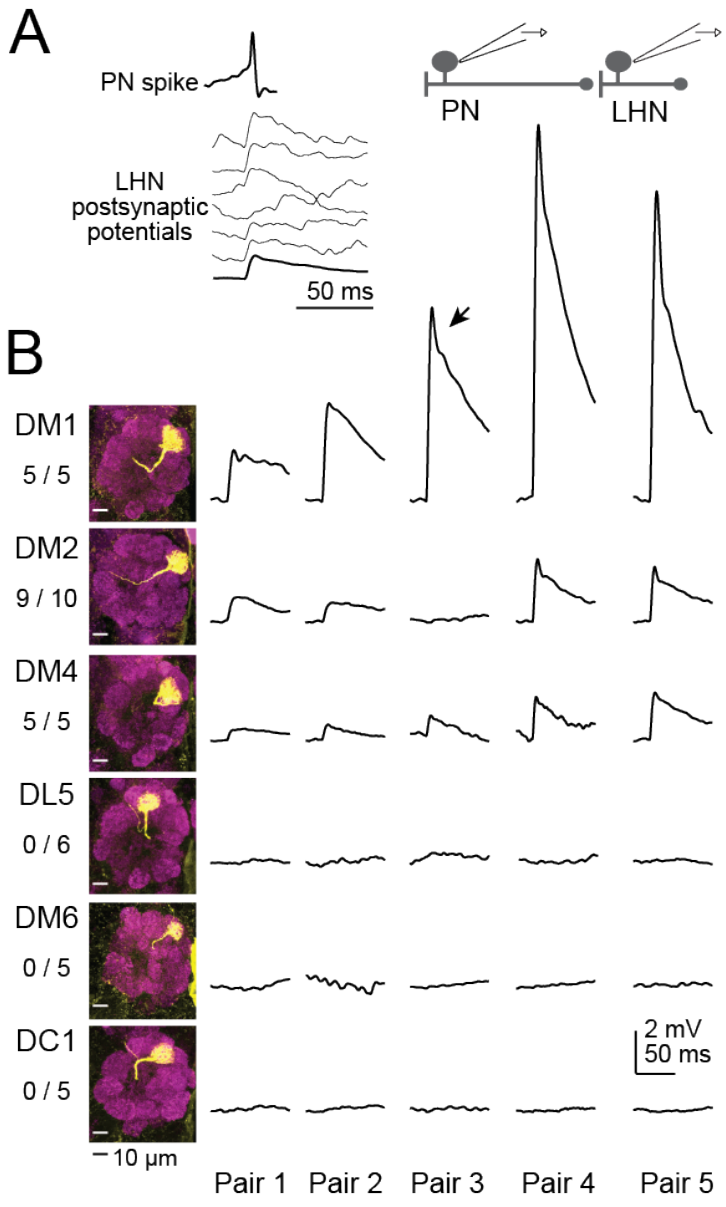

3.4 Integration of excitatory input from multiple glomeruli by type I neurons

The glomeruli that provide input to *Mz671* neurons (DM1, DM2, and DM4) are co-activated by many fruity-smelling organic acetates[7,70]. Therefore, some salient olfactory stimuli (such as fruits) might co-activate these glomeruli. To determine how signals from co-activated glomeruli are integrated in these LHNs, we made simultaneous triple *in vivo* recordings from one *Mz671* neuron and two of its presynaptic PNs, where all three neurons were labeled with GFP. The two PNs were depolarized with current injection so that they fired trains of spikes, either individually or together (Figure 4a).

These experiments revealed that postsynaptic spiking could be driven by a single PN (Figure 4b,c). When PNs spiked at high rates, either individually or simultaneously, the postsynaptic response followed a saturating sigmoid function (Figure 4b,c). Because input from different PNs saturated at different levels, the mechanism of saturation likely resides at the synapse, not the process of spike generation in the postsynaptic neuron.

In trials where both PNs were stimulated, the postsynaptic response was accurately predicted by summing the responses to each input alone (Figure 4d,e). The prediction was generated by fitting sigmoid functions to the trials where single PNs were stimulated individually, and then simply summing the predicted postsynaptic responses to each PN input. This model provided a reasonably good fit to the data (R^2 =0.69; Figure 4e; see also Methods). However, the model did systematically underestimate postsynaptic responses to relatively weak presynaptic inputs. In these cases, one input was often too weak to elicit postsynaptic spikes when stimulated alone, but was strong enough to modestly increase postsynaptic spike rates when co-activated with the second input.

Figure 4. Summing excitatory input from multiple glomeruli.

A. A *Mz671* neuron and two of its presynaptic PNs are recorded simultaneously, where all three neurons are labeled with GFP. In interleaved trials, the PNs are driven to fire either alone or together (using current injection through the patch pipettes), and the responses of the LHN are recorded. The postsynaptic membrane potential is shown for three trials (arrow indicates a spike). The saw-tooth fluctuations (visible especially when DM1 is spiking) are reflect large unitary postsynaptic potentials which time-lock to individual PN spikes.

B. Relationship between PN spike count and LHN membrane potential, where the two PNs are each stimulated in separate trials, not simultaneously. Magenta points are from trials where DM1 PNs were stimulated and blue points are from trials where either DM2 or DM4 PNs were stimulated, depending on the experiment (3 experiments in total). DM2 and DM4 connections had similar strength, and so we pooled data from these glomeruli.

C. Relationship between PN spike count and LHN spike count, where the two PNs are each stimulated in separate trials. Fits are sigmoid functions.

D. Data from all trials, including trials where the two PNs were stimulated separately (magenta and blue), and trials where they were stimulated simultaneously (purple). Hatched surface is a fit to the model.

E. Left, model schematic. Spike rates from each glomerulus are passed through an input-specific saturating nonlinearity, and then summed to generate the LHN firing rate. The input-specific nonlinearities are first fit to single-PN data, and then these same nonlinearities are used to generate the prediction for trials where both PNs were stimulated simultaneously. Right, measured LHN spike counts versus the spike counts predicted by the model. Each point represents a different trial where both PNs were stimulated simultaneously.

Figure 4 (continued): Summing excitatory input from multiple glomeruli

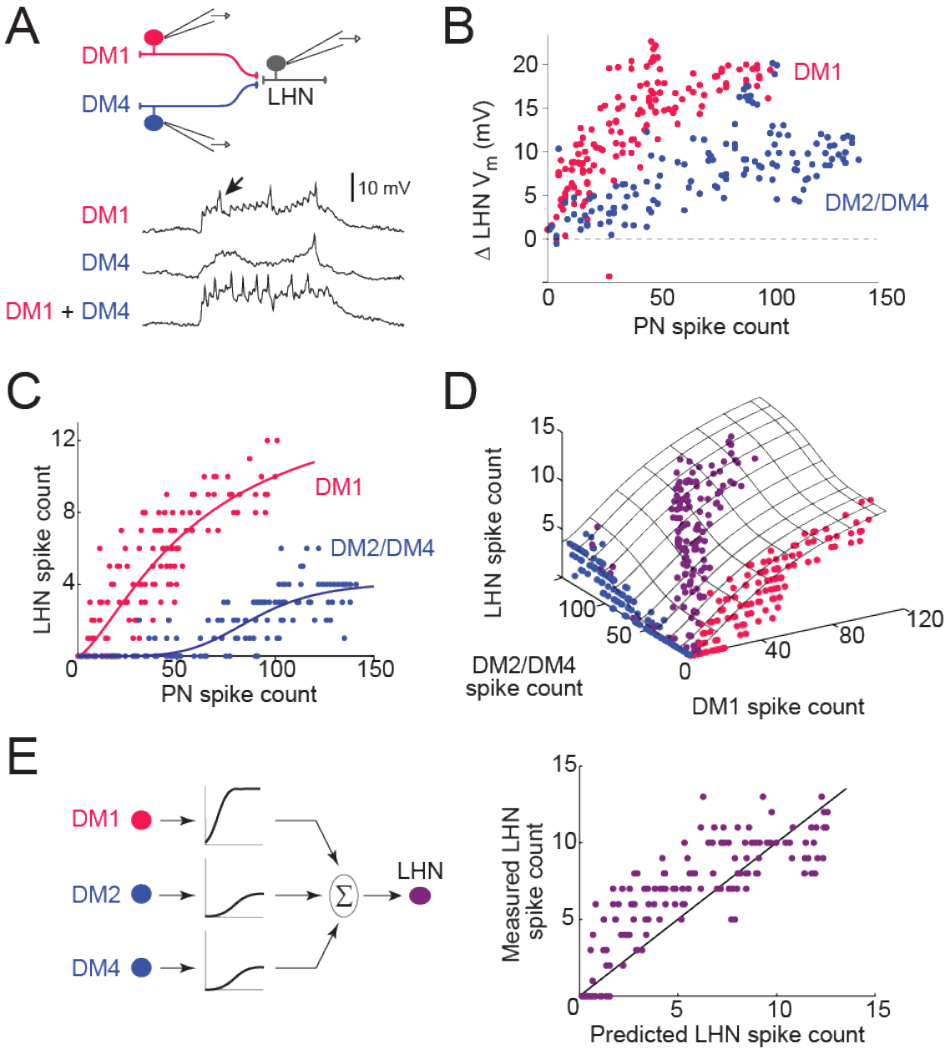

Thus, the inputs to the *Mz671* neurons sum in a fairly linear manner, although they elicit modestly supra-linear postsynaptic responses at weak presynaptic firing rates.

These triple recordings show that a single glomerulus can be sufficient to drive spikes in an LHN, and that recruitment of additional presynaptic glomeruli causes LHN responses to increase further. Based on these results, we predict that LHN odor responses can be driven by odor-evoked spiking in a single presynaptic glomerulus. We also predict that LHN odor responses should increase as additional glomeruli are recruited by an odor stimulus. Summing over glomeruli in this manner could allow LHNs to be sensitive to a broader range of stimuli than any single one of their input glomeruli.

To test these predictions directly, we recorded the odor responses of *Mz671* neurons, DM4 PNs, and DM1 PNs. We focused on one odor (methyl acetate) diluted over a large concentration range. We chose this odor because it activates both DM4 PNs and DM1 PNs, but it activates them at different concentrations; also, this odor is selective for DM4 at low concentrations[18]. As such, this odor allows us to test the specific predictions emerging from our triple recordings. As expected, we found that the *Mz671* neurons were recruited by low concentrations of this odor that are selective for glomerulus DM4 (Figure 5a,b). This confirms that odor responses in a single presynaptic glomerulus are sufficient to drive these neurons. When odor concentration was increased, DM4 PNs were saturated and DM1 PNs were recruited. As expected, LHN responses were sensitive to the recruitment of DM1 PNs: their responses continued to grow although input from DM4 was no longer growing (Figure 5a,b). This result confirms that odor responses in the *Mz671* neurons increase as additional glomeruli are recruited by an odor.

Figure 5. Lateral horn neuron odor responses are sensitive to single glomeruli.

A. Typical *in vivo* whole-cell recordings from a *Mz671* neuron, a DM1 PN, and a DM4 PN (recorded separately). The odor is methyl acetate. Low concentrations recruit DM4 but not DM1. High concentrations saturate DM4 and begin recruiting DM1. LHN responses increase over the entire concentration range.

B. Concentration-response functions. Different points at a single concentration are from different experiments (n=6 for each cell type). Smooth lines are fits to the equation

$$f([odor]) = A\ \frac{1}{1 + \sigma^n/[odor]^n}$$

where [*odor*] is log odor concentration.

C. The fitted parameters which describe the shape of the curve (n and s) are significantly different for DM4 PNs and LHNs (unpaired two-tailed t-tests, *n:* P=0.0017, d.f.=10, *s:* P=0.0076, d.f.=10). Parameter n measures the steepness of the curve and s is the concentration which produces a half-maximal LHN response (in units of –log dilution). The discrepancy between spike counts shown in panel b and Figure 4 is addressed in Figure 6.

Figure 5 (continued): Lateral horn neuron odor responses are sensitive to single glomeruli.

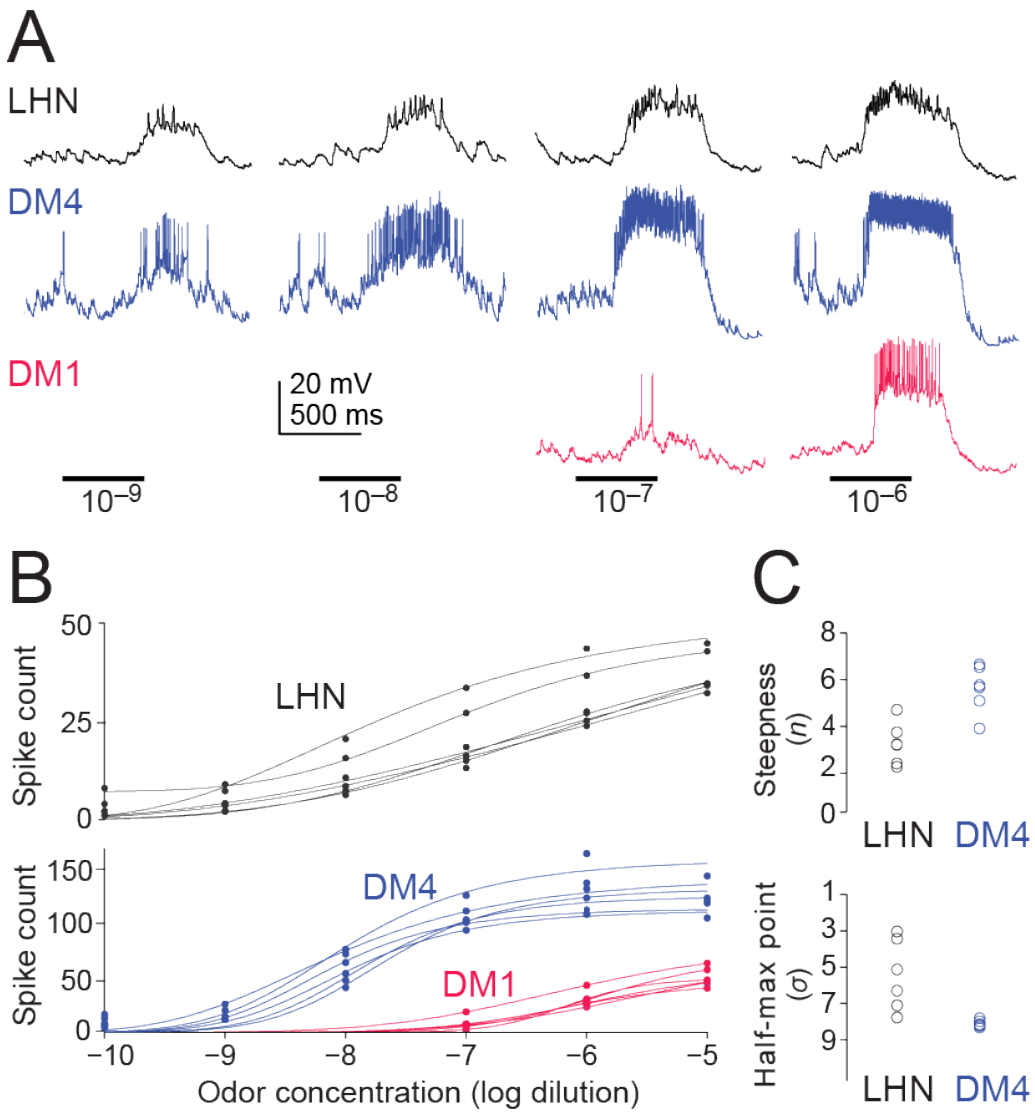

Note that the *Mz671* neurons encode a broader range of concentrations as compared to their individual presynaptic PNs. We quantified this by measuring the steepness of the concentration-response functions; this analysis showed that the LHN responses are significantly less steep (Figure 5c). This finding arises from the fact that the PNs in question are sensitive to different concentration ranges of the same odor. As a result, summing the two PN responses produces a broader dynamic range in the postsynaptic LHNs. Note that PN concentration-response functions are steeper than those of LHNs over a relatively limited portion of the odor concentration range. In addition, the trial-to-trial reliability of PN responses, quantified by the fano-factor, is similar to that of LHN responses, for matched odor-evoked firing rates (data not shown). Thus, PNs are more informative about concentration over a narrow range, but LHNs carry information about a broader range.

The spike counts recorded in Mz671 neurons in triple recording experiments were substantially lower than those obtained in recordings from the same neurons with olfactory stimulation even when the PNs were firing at similar rates (compare Figs. 4 and 5). This discrepancy may be attributable to several causes. First, glomeruli other than DM4 may be recruited by low concentrations of the odor (methyl acetate), and these glomeruli might be presynaptic to these LHNs. If so, then the LHN would fire at a higher rate than we would expect based on the activity of DM4 alone. There is evidence that methyl acetate is specific for DM4 at these concentrations[18], but this idea is still difficult to completely exclude. Second, there could be more than one DM4 PN. If so, we would be stimulating more PNs with odor versus with current injection. This is unlikely, because when we expressed PAGFP pan-neuronally and photoactivated the DM4

glomerulus, we found only one DM4 PN. Third, LHNs may exhibit different excitability in the two types of experiments.

In support of the idea that postsynaptic excitability accounts for the discrepancy, there was a systematic difference in the stimulus-evoked change in LHN spike rate for a given change in LHN membrane potential across the data sets (Figure 6a). Moreover, both spontaneous EPSPs and spikes were systematically reduced in the triple recordings relative to odor delivery experiments (Figure 6b and c; each point in panel b is a different experiment). In the triple recordings, we hyperpolarized the two PNs below their normal resting potential, thereby preventing them from spiking outside the stimulation window. In any given triple recording, we are thereby silencing two of the four known PN inputs to the LHN. This likely explains why spontaneous EPSPs are suppressed. In sum, we conclude that the LHN dendrites are likely somewhat hyperpolarized in the triple recordings, due in part to reduced spontaneous PN input, which diminishes the recruitment of voltage-dependent conductances in LHNs, thereby decreasing postsynaptic depolarization in response to PN spikes, and inhibiting postsynaptic spike generation.

Figure 6. Spontaneous activity modulates excitability in Mz671 neurons

A. Stimulus evoked membrane potential to stimulus evoked firing rate relationship for Mz671 neurons under two experimental conditions with two different stimuli. Blue, LHN recordings from odor delivery experiments. Red, LHN recordings from triple recordings. LHN spikes were detected, counted and then filtered out by low pass filtering the membrane potential. Vm calculation for triplet data was performed as described in Chapter 2.6.2. For odor response data, we used variable windows over which to calculate membrane potential deviation, because odor response magnitude and delay are correlated.

B. Spontaneous spiking in Mz671 LHNs under two experimental conditions. Color scheme as in panel a.

C. Membrane potential recordings displaying spontaneous EPSPs in single trials from three different neurons each under two experimental conditions. Color scheme as in panel a.

Figure 6 (continued): Spontaneous activity modulates excitability in Mz671 neurons

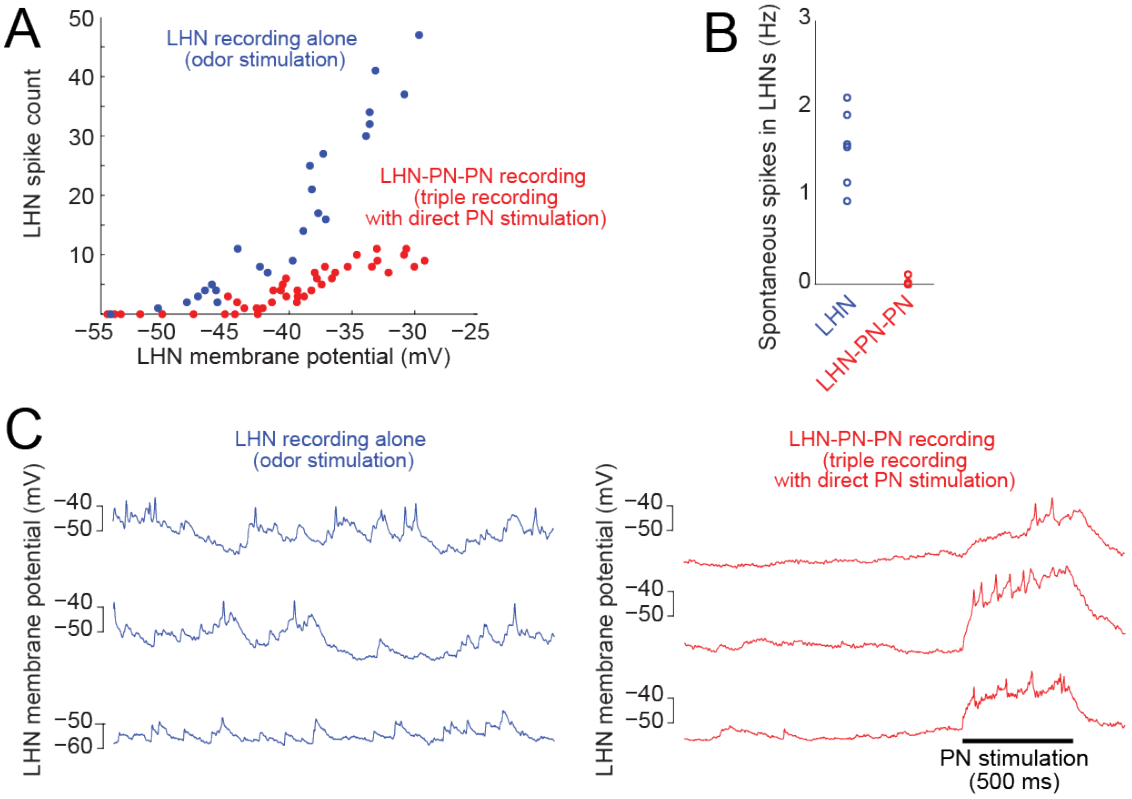

This finding indicates that the adaptation state of the postsynaptic neuron is different in the two experimental conditions. Therefore we must interpret these results cautiously with regards to the linearity of integration. In both experiments we find that individual inputs are sufficiently strong to elicit postsynaptic spiking, and that multiple inputs sum effectively. The triple recordings reveal integration that can be accounted for with a relatively simple linear summation rule, but the data does not explore a more excitable region of the conductance space of the postsynaptic neuron. Therefore it could be that spontaneous synaptic input depolarizes the postsynaptic neuron and carries it into a state where stronger supralinearities in summation appear. The odor concentration series presented in figure 5 does not reveal any strong evidence to favor this possibility. However, the experiment of figure 5 is not a strong test of this hypothesis, as coactivation of inputs is limited to the region of input space where one input is saturated. In this regime, summation appears compatible with a linear rule. However it is possible that co-activation of inputs at levels where neither input is saturated might reveal facilitatory interactions. This region of the transformation can be explored with further triple recordings where spontaneous activity is controlled to resemble the conditions found in odor delivery experiments.

3.5 Connectivity from glomeruli onto type II neurons

Next, we investigated connectivity onto the *NP6099* neurons (type II). Overall, type II neurons are more narrowly tuned than type I (Figure 2), suggesting they receive excitation from fewer glomeruli. Indeed, we found zero connections in 82 paired recordings from randomly-selected PNs and *NP6099* neurons. As there are only 49

glomeruli in total, this connection rate raises the possibility that the *NP6099* neurons receive PN input from only one glomerulus.

A previous study predicted that the *NP6099* neurons receive direct input from glomerulus DP1m and glomerulus VA2, because their dendrites overlap with the projections from these glomeruli[13]. Because there is no available Gal4 line selective for the PNs in either of these glomeruli, we used an alternative approach to target these PNs for paired recordings (Figure 7a). Namely, we expressed PA-GFP under the control of a Gal4 line expressed in many PNs, and we photoactivated specifically in the glomerulus of interest. This allowed us to target our electrodes selectively to PNs in either DP1m or VA2. We filled each recorded PN to confirm its identity *post hoc*.

Using this approach, we performed four paired recordings with DP1m PNs and *NP6099* neurons. In all four cases, we found a connection. By contrast, we observed no connection with glomerulus VA2 in six of seven experiments, although there was a weak connection in one experiment (Figure 7b). This example suggests that there are small variations in the wiring of connections from PNs onto LHNs, perhaps due to developmental errors (see also the "missing" connection in Figure 3b, second row). Nonetheless, the overall conclusion from these recordings is that connectivity is highly selective. In particular, it is notable that the VA2 PNs do not form connections with the *NP6099* neurons, although their axons and dendrites exhibit considerable overlap[53].

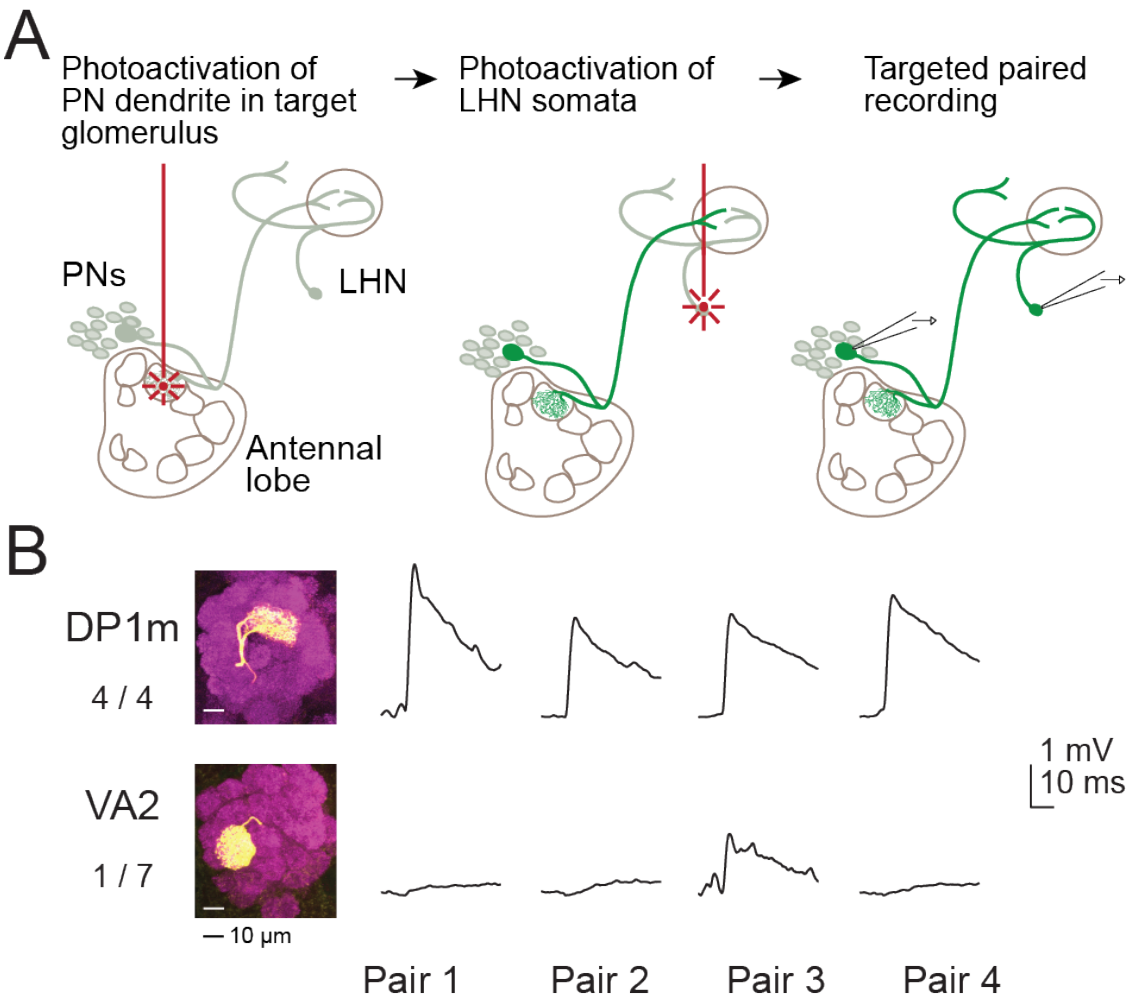

Figure 7. Paired recordings identify excitation from one glomerulus.

A. Paired *in vivo* recordings guided by PA-GFP. PA-GFP was expressed in many PNs (under the control of *GH146-Gal4*) and in *NP6099* neurons. We photoactivated in a single glomerulus (either DP1m or VA2) to label the corresponding PN soma. We next we photoactivated the *NP6099* neuron somata, and then simultaneously recorded from a PN and a LHN.

B. Results from multiple experiments of this type (see Figure 3b legend). Four of four DP1m pairs showed a connection. Only one of seven VA2 pairs showed a connection and this response was unusually weak.

3.6 Gating of feedforward excitation in type II neurons

Identifying presynaptic antennal lobe PNs for the *NP6099* neurons allowed us to compare the odor tuning of these synaptically connected PNs and LHNs. We found that every test odor that activated the LHNs also activated the DP1m PNs (Figure 8a,b). This is consistent with the idea that the *NP6099* neurons receive most or all of their excitation from DP1m. In further support of this idea, we found that the input from DP1m is strong enough to account for the size of the excitatory odor responses in the LHN. Specifically, in paired recordings, direct current injection into DP1m PNs elicited a LHN response that matched the odor-evoked response to the same odor-evoked PN firing rate (Figure 8a). Thus, DP1m may be the only glomerulus that provides direct excitatory input to the *NP6099* neurons.

Interestingly, some odors elicited a robust response in DP1m PNs but little or no postsynaptic spiking in the *NP6099* neurons. This suggests that excitatory input from DP1m is gated by strong, odor-selective inhibition from co-activated glomeruli. For example, whereas both octanoic acid and E2-hexenal elicit a robust PN response, only octanoic acid elicits a response in the LHNs (Figure 8a,b). This suggests there is a glomerulus which is activated by E2-hexenal but not octanoic acid, and inhibition from this glomerulus gates the excitation arising from DP1m.

Figure 8. Odor-selective inhibition gates excitation from glomerulus DP1m.

A. Odor responses of *NP6099* neurons plotted against responses of DP1m PNs. Each point is an odor stimulus (mean ± s.e.m. computed across experiments, n=4 - 13 PNs and 4 - 17 LHNs per point, odors shown in Figure 9). The lower panel shows data from a separate set of experiments (paired recordings from DP1m PNs and *NP6099* neurons) where the PN was directly depolarized to fire trains of spikes via current injection through the patch pipette (n=2 pairs, pooled trials binned by PN spike rate, averaged within a bin, and fit with an exponential). These paired recordings show that synaptic excitation from DP1m is strong enough to account for the strongest odor responses of *NP6099* neurons (see gray fitted function in top panel reproduced from lower panel).

B. Odor responses of DP1m PNs and *NP6099* neurons to octanoic acid and E2-hexenal (both 10^{-2}). Rasters above each trace show spikes. Although these two stimuli elicit similarly strong responses in DP1m PNs, the postsynaptic response to E2-hexenal is selectively suppressed.

C. Both responses are disinhibited by the *Orco* mutation (which also eliminates the difference between the responses) and attenuated by the *Ir64a* mutation. The plot below quantifies responses to several stimuli in wild type flies, *Orco* mutants, and *Ir64a* mutants (± s.e.m.). For both genotypes, the effect across all odors was significant (n = 4 - 6 experiments per odor for each mutant and 9 - 17 experiments per odor for wild type, 2-way ANOVA,F_{IR64a} (1,77)=9.25, P=0.0032, F_{ORCO}(1,71)=719.43, P=3.63×10^{-5}).

Figure 8 (continued): Odor-selective inhibition gates excitation from glomerulus DP1m.

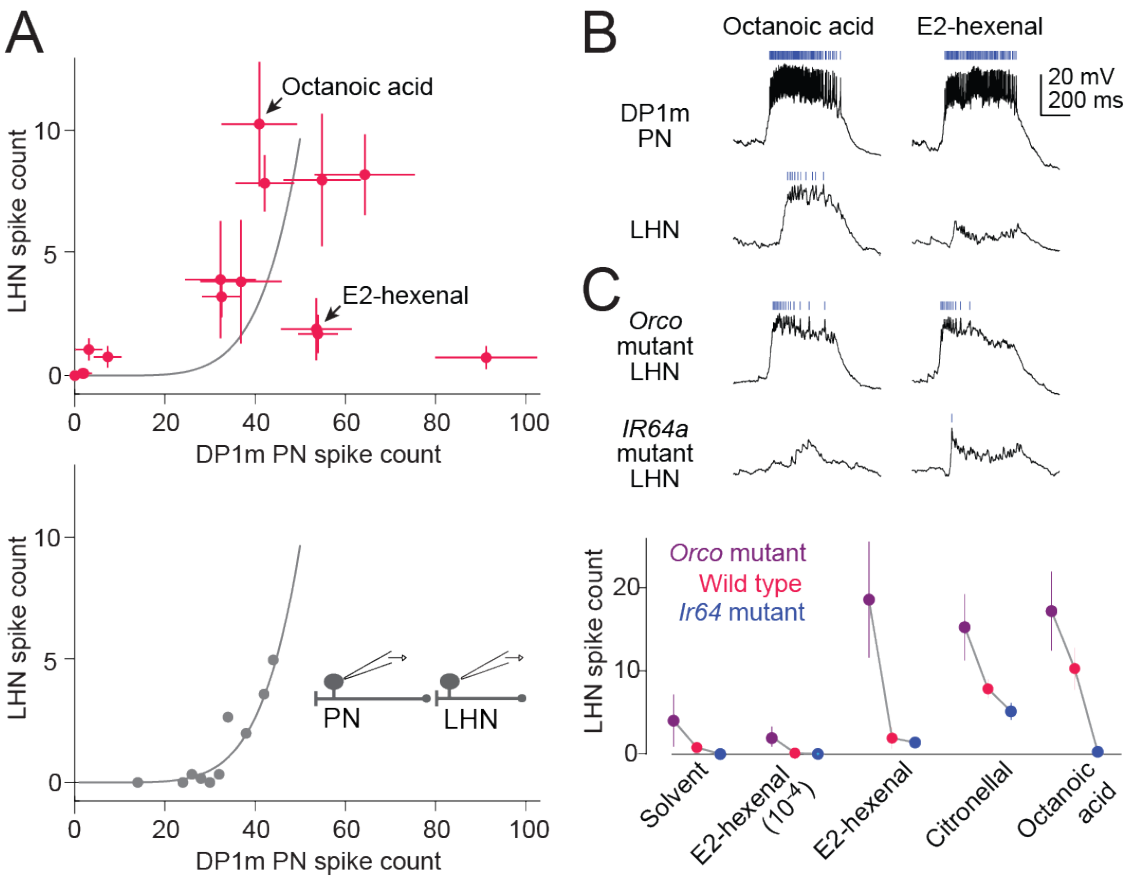

To further explore the origins of inhibition, we recorded from these same LHNs in *Orco* mutants. The *Orco* gene encodes a co-receptor which is expressed by most olfactory receptor neurons[64]. Many olfactory receptor neurons are *Orco*-positive, and in these neurons, *Orco* is absolutely required for olfactory transduction[64]. However, DP1m olfactory receptor neurons do not require *Orco* for normal transduction[71]. We found that the *Orco* mutation disinhibited odor responses in the *NP6099* neurons (Figure 8c). This result indicates that one or more *Orco*-positive glomeruli are the source of inhibition in these LHNs.

Conversely, odor responses in *NP6099* neurons were reduced by a mutation in *Ir64a*. The *Ir64a* gene encodes an odorant receptor which is expressed by DP1m olfactory receptor neurons and is necessary for their normal function[65]. This mutation does not completely abolish odor responses in the DP1m olfactory receptor neurons [G. Suh, personal communication], and so the residual odor responses we observe in the mutant are compatible with the conclusion that DP1m is the only source of direct excitation to the *NP6099* neurons. Together, these two mutations indicate that odor-specific inhibition from *Orco*-positive glomeruli gates excitation from glomerulus DP1m.

Because inhibition is tuned, it likely arises from a small number of glomeruli, rather than the summed activity of many glomeruli (Figure 9). Note that the largest relative suppression in the LHN response (relative to the DP1m response) is observed for E2-hexenal (10^{-2}), valeraldehyde (10^{-2}), and 2-butanone (10^{-2}). By comparison, relatively little suppression is observed for 1-penten-3-ol (10^{-2}) and 1-octen-3-ol (10^{-2}). There is no systematic relationship between the amount of suppression and the amount of total activity elicited in ORNs.

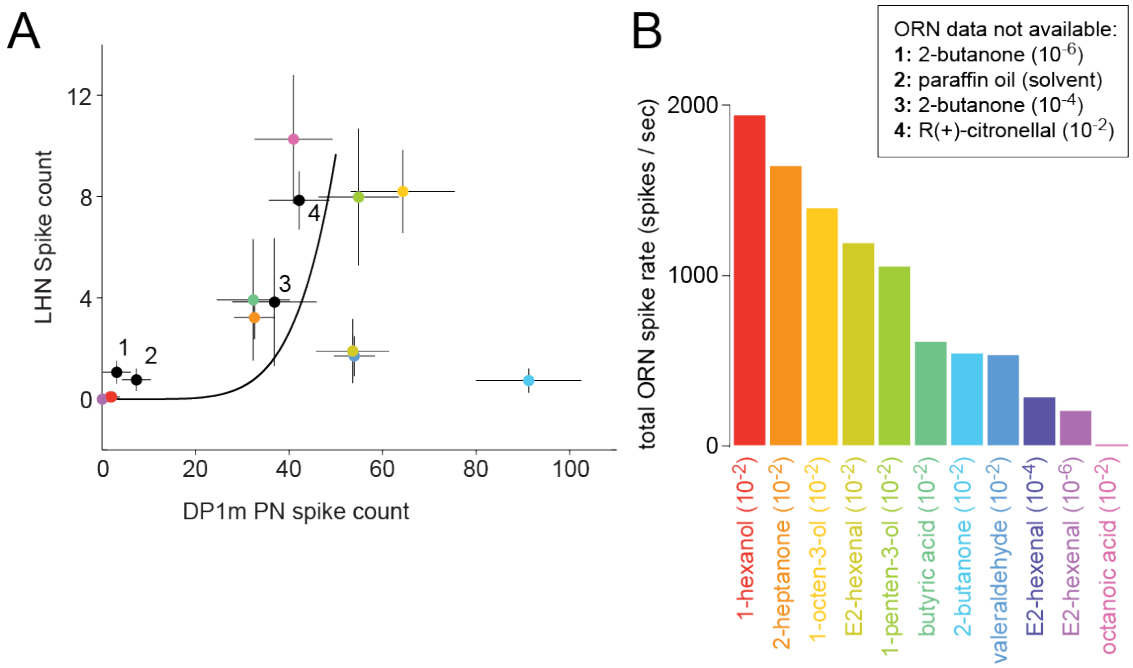

Figure 9. Inhibition in NP6099 neurons does not depend on total network activity.

A. This panel contains the same data as in Figure 8a (top, magenta symbols), but with stimuli color-coded. The smooth curve reproduces the fitted line from Figure 8a (bottom).

B. The total amount of olfactory receptor neuron activity for each stimulus, obtained by summing across the firing rates for all receptor types measured by Hallem et al. 2006[7]. Color codes are the same as in panel a. (For the four numbered stimuli in black from panel a, olfactory receptor neuron data are not available.)

Thus, the inhibition which suppresses these responses must be selective for the chemical composition of an odor (presumably therefore reflecting input from a small number of glomeruli), and is not simply driven by total network activity.

3.7 Circuit origins of inhibitory inputs to type II neurons

What inhibitory neurons relay odor-specific inhibition to these LHNs? Likely candidates are the GABAergic inhibitory antennal lobe PNs (iPNs). [9–11] These PNs project through an axon tract which is separate from the tract carrying the axons of excitatory PNs (ePNs), so we could use two-photon laser-transection to selectively cut the axons of ePNs, leaving iPN axons intact (Figure 10a). This manipulation abolished excitation in the *NP6099* neurons, revealing pure inhibition (Figure 10b). This residual inhibition likely originated from iPNs, because it disappeared when we cut both the iPN axon tract and the ePN axon tract (Figure 10b). However, this residual inhibition was weak, and when we cut the axons of iPNs rather than the axons of ePNs, we observed little to no disinhibition (Figure 10b,c), especially as compared to the effects of the *Orco* mutation (Figure 8c).

Figure 10. Circuit origin of inhibition: direct GABAergic projections

A. Two inhibitory circuits: one via GABAergic inhibitory PNs (iPNs) in the antennal lobe, the other via GABAergic local neurons in the lateral horn. The axon tracts of iPNs and excitatory PNs (ePNs) are segregated and so can be cut selectively.

B. Odor responses of DP1m PNs and *NP6099* neurons (top trace is reproduced from Figure 7b). Cutting ePN axons eliminates excitation and reveals inhibition (cells were held at a depolarized potential to better show inhibition; note different vertical scale in this row; similar results in 9 experiments). However cutting iPN axons does not completely abolish inhibition (compare with the *Orco* mutation, Figure 7c). Cutting both tracts eliminates all odor responses.

C. Odor responses of *NP6099* neurons in experiments where iPNs were intact (data from Figure 7) or cut (n=6, ± s.e.m.). There is no significant effect on spike counts (2-way ANOVA, $F_{iPNcut}(1,67)=0.45$, $P=0.51$), although subthreshold responses were often partly disinhibited.

Figure 10 (continued): Circuit origin of inhibition: direct GABAergic projections

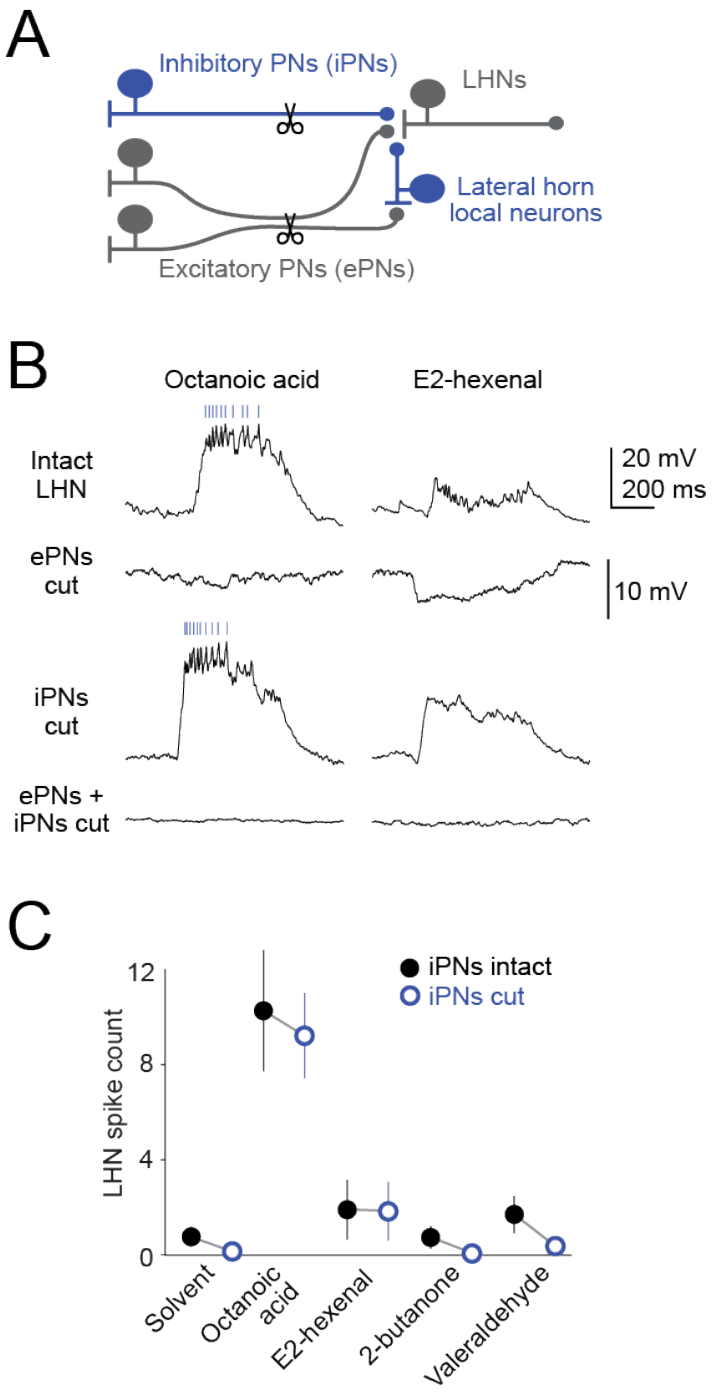

Together, these results imply a second source of inhibition, in addition to the inhibition arising from iPNs. The logical candidate would be GABAergic neurons in the lateral horn itself (Figure 10a). Therefore, we performed a GABA immunostain and found a cluster of GABAergic somata adjacent to the lateral horn (Figure 11a). We identified a Gal4 line which labels these neurons, and we patched and filled individual labeled cells from this line. This confirmed that these neurons have purely local arbors (Figure 11b). Interestingly, we observed that all the neurons we recorded from had narrow odor tuning (Figure 11c-e). Thus, these local neurons are well-positioned to provide odor-specific inhibition.

In sum, these results provide evidence that inhibition arises from two sources. Some inhibition arises from a direct GABAergic projection from the antennal lobe, and additional inhibition likely arises from a local GABAergic circuit within the lateral horn. Although inhibition is much more prominent in type II neurons, it can occasionally be seen in type I neurons as well (Figure 12).

Figure 11. Circuit origin of inhibition: GABAergic local neurons in the lateral horn.

A. Single confocal sections through the lateral horn of a brain triple immunostained for neuropil (nc82), CD8, and GABA. Dorsal is up, lateral is right. Expression of CD8:GFP is driven by a Gal4 line with a restricted expression pattern (GMR23F06-Gal4). In the overlay, a magenta circle indicates the approximate boundary of the lateral horn (as in panel B). Similar results were obtained in three brains.

B. Sample morphologies of lateral horn local neurons, traced from biocytin fills. Similar fills were obtained for a total of 7 cells. A few of these neurons have local arbors that extend beyond the boundaries of the lateral horn (e.g., the second example here). The morphology of a type II LHN is shown for comparison (reproduced from Figure 1).

C. Odor responses of a GABAergic lateral horn local neuron.

D. Odor selectivity of a population of lateral horn local neurons. Spikes are counted over a duration of 1 s starting at the odor onset command. Each line connects spike counts from the same neuron (n=7; some cells do not spike in response to any odors but all displayed subthreshold responses).

E. Lifetime sparseness of odor-evoked spike rates in type I and II neurons (same cells as Figure 2a,b) and lateral horn LNs (n=5 cells, same as panel D, except cells that did not spike in response to either current injection or odor are omitted). Each symbol represents a different experiment. A sparseness of 1 is maximally selective, 0 is nonselective. One LN and one type II neuron spiked in response to current injection but not odor and were assigned a sparseness of 1. Note that the spiking responses of lateral horn LNs are highly selective.

Figure 11 (continued): Circuit origin of inhibition: GABAergic local neurons in the lateral horn.

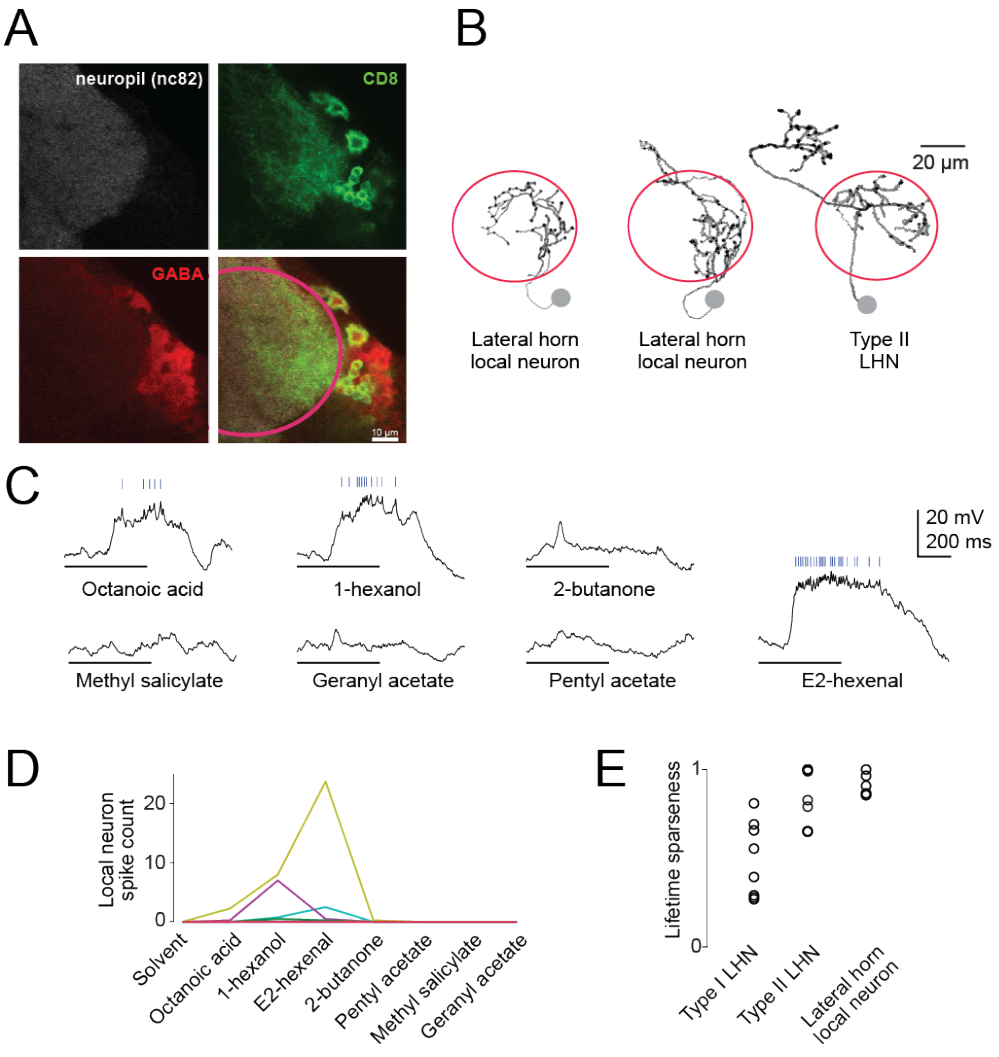

Figure 12. Type II LHNs, but not type I LHNs, receive prominent odor-evoked inhibition.

A. Responses of a typical NP6099 neuron to a stimulus that elicits prominent hyperpolarization. In different trials, we manipulated the membrane potential of the LHN by injecting different amounts of current via the patch pipette. Note that odor-evoked hyperpolarization increases at more depolarized holding potentials, indicating that inhibition is at least partly postsynaptic.

B. In a single case, we observed odor-evoked hyperpolarization in a type I LHN. This was noted as part of our general survey of type I LHNs labeled by GMR48F03-Gal4 and GMR73B12-Gal4 (Figs. 1c and 2a). In addition to the core odor set shown in Figure 2a, we used 26 additional odors in various recordings in the course of this survey, in order to determine if any of them elicited hyperpolarization. We held cells at a depolarized potential during these trials (-40 to -30 mV) to better reveal any inhibition that might be present. Shown here are responses to these 26 odors, only the last of which elicited any hyperpolarization. This example shows that type I cells can receive odor-evoked inhibition, but is still consistent with the conclusion this inhibition is much less prominent than in type II cells. (Odors are : 2,3-butanedione, 2-heptanone, 2-octanone, 3-octanol, α-pinene, benzaldehyde, butyric acid, cis-3-hexen-1-ol, beta-citronellal, cyclohexanone, ethyl butyrate, ethyl caproate, ethyl cinnamate, ethyl lactate, ethyl propionate, fenchone, g-octalactone, ginger oil, hexyl acetate, linalool, nerol, phenethyl acetate, pyrrolidine, triethylamine, valeraldehyde, isoamylamine; all dilutions are 10-2; horizontal bar in first panel shows 500 ms odor stimulus period.)

Figure 12 (continued): Type II LHNs, but not type I LHNs, receive prominent odor-evoked inhibition.

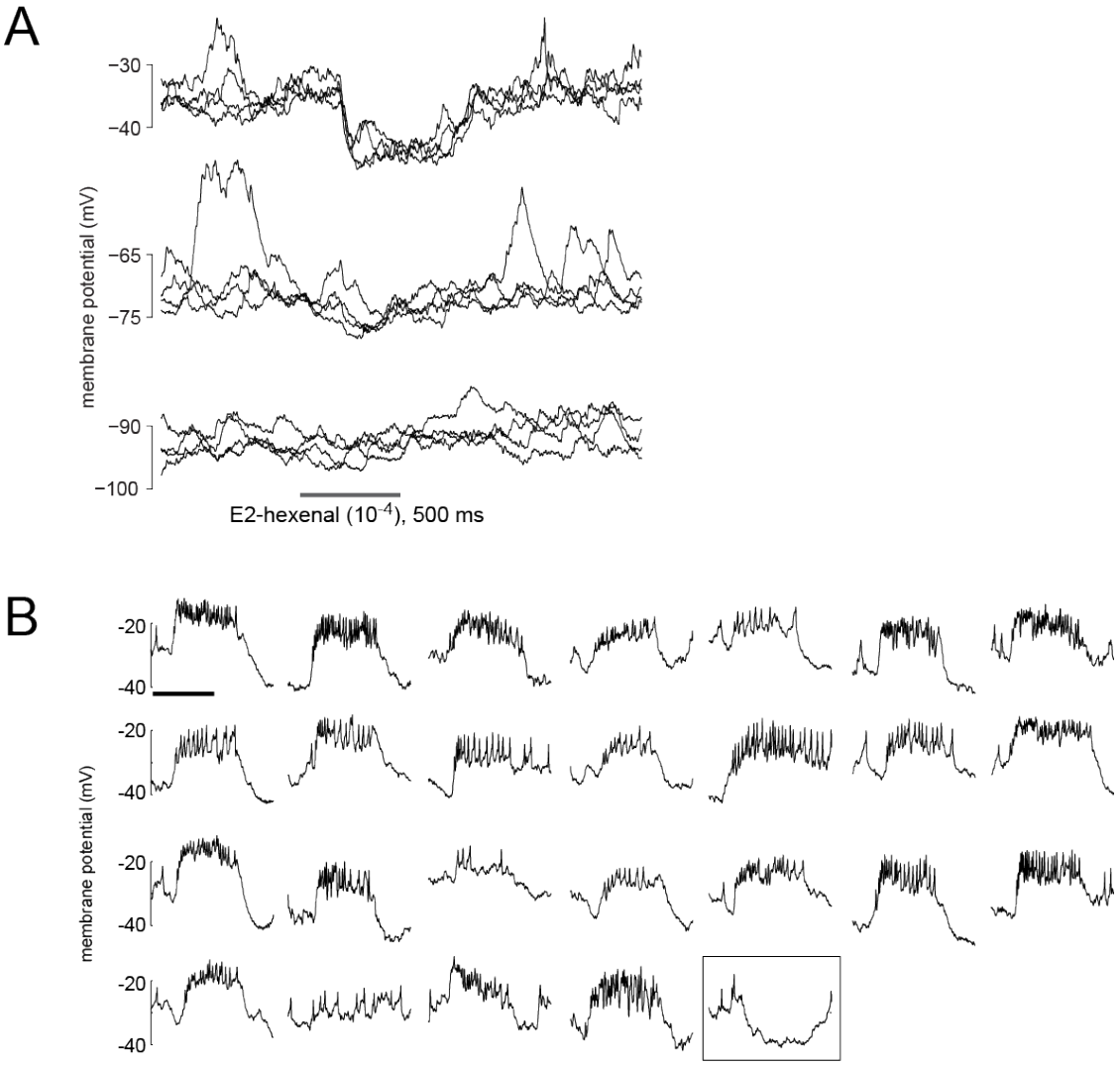

3.8 Discussion

3.8.1 Connectivity onto two types of lateral horn neurons

In order to understand higher olfactory processing, it is fundamentally important to describe how information distributed across many glomeruli is integrated by a typical higher order neuron. A first step in understanding this process is to elucidate how many glomeruli provide input to a typical higher-order neuron. It is also important to know whether these connections are stereotyped. This is important both for evaluating current theories of functional specialization in higher olfactory areas, and for determining the feasibility of our approach to understanding higher olfactory receptive fields.

We used large numbers of paired recordings to map the connectivity of representative lateral horn neurons. In accordance with the stereotyped odorant selectivity of individual lateral horn neurons, we found that their connectivity is also stereotyped. Furthermore we found that different glomerular inputs are associated with different and stereotyped synaptic weights, and that some combinations of glomeruli occur preferentially. These findings reveal differences between the mushroom body and lateral horn, and indicate that our approach is feasible.

First, our random samples of PN-LHN pairs allow us to estimate the number of input glomeruli for each LHN type. For our representative type I neurons (the *Mz671* neurons), we performed 120 paired recordings with random PNs and found 5 connections. Given 49 glomeruli[8], binomial statistics would indicate with ~95% confidence that there are at most four connected glomeruli. Indeed, we identified four inputs for these neurons (DM1, DM2, DM4, VA7l). This calculation assumes that there are equal numbers of PNs in all glomeruli. In total there are ~150 PNs[72], which would

predict three PNs per glomerulus, but it is known that some glomeruli contain more than three (e.g., glomerulus DA1[73]) and some contain only one[19]. If a glomerulus contained only one PN, then we would be more likely to miss it, and indeed glomerulus DM1 was a near miss: it contains one PN[19], and it did not turn up in our random screen; we identified it only as a result of our targeted paired recordings. There might also be additional deviations from random sampling in our untargeted PN recordings. While we have sampled extensively from both clusters of excitatory PN cell bodies, there might nonetheless be biases against sampling some relatively less accessible PNs. Thus, four glomeruli might be an underestimate. Nonetheless, it seems likely that each type I neuron receives input from fewer than ten glomeruli.

For our representative type II neurons (the *NP6099* neurons), we performed 82 paired recordings with random PNs and found zero connections. Binomial statistics would indicate that there are at most two connected glomeruli, with the same caveats as above. However, for these neurons, there is independent evidence arguing that DP1m is the only excitatory input. Specifically, all the odors that activate these neurons also activate DP1m PNs, and the firing rates of DP1m PNs are sufficient to predict the strongest odor responses in these neurons. It will be interesting to learn if all type II neurons receive excitatory input from a single glomerulus. It is notable that VA2 PNs do not connect to these neurons, despite substantial axon-dendrite overlap[53]. These results raise the question of how a lateral horn neuron reliably forms a connection with one axon but avoids forming a connection with another axon, in a case where the two axons are overlapping.

An important conclusion of our study is that some glomerular combinations are substantially over-represented in the lateral horn. Consider the fact that there are three *Mz671* neurons per lateral horn, but only several hundred lateral horn neurons in total (based on cell counts in experiments where we expressed PA-GFP pan-neuronally and photoactivated in a large volume of the lateral horn; Figure 1a). We identified 4 glomeruli connected to *Mz671* neurons. Given 49 glomeruli in total[8], there are >200,000 possible combinations of four glomeruli. This is far larger than the total number of neurons in the lateral horn. Moreover, the particular glomerular combination sampled by the *Mz671* neurons occurs not once, but at least three times in every lateral horn. Therefore, the space of possible glomerular combinations is sampled non-randomly.

Paired recordings also show that different glomerular inputs to an LHN can be associated with non-uniform and stereotyped synaptic weights. This has been proposed previously as a way to render LHNs more selective for a particular olfactory feature[34]. This too indicates a high level of precision in the development of this circuit.

In many of these respects, our results show that the lateral horn differs radically from the mushroom body, the other third-order olfactory region in insects. In the mushroom body, the pattern of glomerular inputs to the mushroom body appears to be different in different individuals[49,53,74,75]. And although there are regional biases in connections from glomeruli to the mushroom body[48,76] and glomeruli with similar tuning tend to wire together[43], connectivity in the mushroom body nonetheless seems to be probabilistic rather than deterministic. This contrasts with the highly stereotyped wiring we found in the lateral horn.

Ablating the mushroom body impairs learned but not unlearned olfactory discriminations. This observation was taken to suggest that the lateral horn is sufficient for innate olfactory behavior[50,52]. Our finding of stereotyped connectivity supports the notion that the lateral horn performs a sensory function which is less variable across individuals in comparison to the mushroom body. It should be noted that the stereotypy we observe may be entirely specified by the genetic inheritance of these organisms, but this need not be the case. All the flies we used in our experiments were raised in a similar environment. Future studies will be needed to know whether there is any experience-dependent element in these connections or their weights.

3.8.2 Odor coding and computations in lateral horn neurons

Our results demonstrate that different types of lateral horn neurons carry out distinct computations on the information they receive from olfactory glomeruli. Type I neurons are broadly tuned to odors, and the *Mz671* neurons are typical of type I in this respect. Consonant with this, we found that the *Mz671* neurons neurons pool excitation from a handful of co-activated glomeruli, and input from even a single glomerulus can be sufficient to drive postsynaptic spiking. This shows that input integration occurs differently in the lateral horn and the mushroom body, where multiple inputs have to be active to drive postsynaptic spiking. Due to the efficacy of single inputs, we might expect these LHNs to be more broadly tuned to odors than PNs are. Broad odor tuning to a group of related chemicals might be a useful way to link a large region of chemical space (e.g., odors associated with fruit) with an innate behavioral program (e.g., feeding).

In addition, we observed that the *Mz671* neurons have a broader dynamic range for concentration encoding, as compared to their presynaptic PNs. *Drosophila* can generalize across different concentrations of the same odor, and this behavioral performance requires integrating activity across multiple glomeruli that are co-activated by some odors, but with different sensitivities to those odors[77,78]. Whereas each individual glomerulus can only encode concentration over roughly two orders of magnitude, summing several glomeruli having different dynamic ranges can yield a broader range of sensitivity[77]. This is precisely what the *Mz671* neurons do. Thus, type I LHNs might play a role in concentration generalization.

In contrast to type I, type II neurons are narrowly tuned, and the *NP6099* neurons are typical of type II neurons in this respect. Again, consonant with their narrow tuning, we showed that the *NP6099* neurons combine excitation from one (or a few) glomeruli with tuned inhibition from co-activated glomeruli, yielding greater selectivity. This represents a computation which is distinct from that performed by the *Mz671* neurons. On theoretical grounds, combining excitation and inhibition from co-activated glomeruli has been proposed previously as a way to generate selectivity[34]. Behavioral data shows that *Drosophila* can perform fine discriminations among odor stimuli with different chemical compositions[77,79]. Neurons with high selectivity might be a useful way to link specific odor stimuli with behavioral programs.

Chapter 4.

High throughput mapping of connectivity in the *Drosophila* olfactory system

4.1 Introduction

In the last chapter we presented evidence that lateral horn neurons sample non-randomly from small subsets of olfactory glomeruli. A natural question to ask is the following: is there any special relationship in the chemical tuning of the glomeruli that are pooled together? We found that for both type I and type II neurons, the glomeruli that are pooled together overlap in their chemical tuning. In type I neurons, we found that summation over similarly tuned glomeruli can produce a broader dynamic range for encoding the concentration of odorants. These are odorants for which these glomeruli have slightly different sensitivity. In type II neurons, we found that a subtractive operation performed over similarly tuned glomeruli can produce a tuning profile more selective for particular odorants.

These findings describe the "form" of the transformation of olfactory representations in the lateral horn. The sign and effectiveness of each input, combined with the degree of tuning overlap, determines the output. However they do not inform us about the "content" of what is computed: which actual odorants, or odorant features are extracted through these computations? This is a difficult question to answer. However we think we can take a step towards answering it by investigating the patterns in feedforward connectivity going from the antennal lobe to the lateral horn.

Given that there are ~50 glomeruli, and assuming that every lateral horn neuron receives inputs from ~4 glomeruli, there are more than 200,000 possible combinations of glomeruli that lateral horn neurons could perform. However there are only a few hundred lateral horn neurons in total, and we find that certain combinations of glomeruli are overrepresented. Clearly, not every combination is performed. Only certain regions of stimulus space are summed or subtracted from each other. This is the case in other systems as well. For example, simple cells in primary visual cortex perform combinations over lateral geniculate receptive fields that are localized in space and that lie on a line[1,2]. Therefore the relationship between the tuning curves of glomeruli that are either summed or subtracted are a reflection of the way these receptive fields tile and parse the stimulus space. We would like to better understand the rules that determine which combinations over glomeruli are performed and the significance of these rules in terms of olfactory stimulus space.

What might the relationship between the selected glomerular tuning profiles look like, and what might its significance be in terms of olfactory stimulus space? For example, let's consider a hypothetical population of type II lateral horn neurons. We might find that for each neuron there is one strong excitatory and one strong inhibitory glomerulus that provides input. We can then ask: across the population, what is the nature of the overlap in tuning of the excitatory and inhibitory inputs? It might turn out that inhibitory inputs are tuned to stimuli that reside on the flanks of the excitatory tuning curves. Generally speaking, odorants at the center of the tuning curve of a glomerulus, or in other words the "preferred" odorants of a glomerulus, are odorants that have high affinity for the receptor corresponding to that glomerulus. Odorants that reside on the

flanks of the tuning curve are odorants that have lower affinity for that receptor. These lower affinity odorants will elicit responses only when they are present at a high concentration. Therefore the tuning curve of a glomerulus broadens as the concentration of odorants increases, just as the frequency tuning curve of an auditory neuron broadens as the sound intensity increases.[80] In the event that inhibition is tuned to the flanks of the excitatory tuning curve, we might reason that one potential function for type II-like computations is to generate selective signals in the face of tuning curve broadening with increasing concentration. By delivering inhibition tuned to the flanks of the excitatory input tuning, the ambiguity introduced by high concentration stimuli can be counteracted.

Alternatively, we might find that inhibitory inputs have the same preferred stimuli as excitatory inputs. In other words, odorants that have high affinity for the receptor corresponding to the excitatory glomerulus might also have high affinity for the receptor corresponding to the inhibitory glomerulus. These receptors might still differ in their lower affinity ligands. In this case a subtraction would generate selective signals for odorants that reside on the flanks of the excitatory tuning curve. This might indicate an alternative potential function for type II-like computations: to generate a selective response to an odorant for which there exists no high-affinity receptor in the repertoire of the fruitfly. These examples are meant to illustrate some ways in which lateral horn neurons as a population might be specialized to deal with the particular issues posed by the statistics of odor response profiles in the receptor population. While not exactly "olfactory features" these are statistical features of the transduced olfactory signal.

With such data we would further be in a position to identify patterns in connectivity and relate them to olfactory stimulus space. For example, we might find, for

a hypothetical population of type II lateral horn neurons, that a small collection of glomeruli are highly overrepresented in the population of excitatory inputs, whereas other glomeruli are much more often found as inhibitory inputs. This might indicate that as a population, lateral horn neurons create asymmetric, gate-like relationships between certain larger but stereotyped regions of stimulus space. We could then ask if there are generalities about these excitatory vs. inhibitory glomeruli in terms of the odorants they are responsive to. We could further ask if the odorants extracted by these operations have any shared properties in their environmental distribution that illustrates their importance to the animal.

4.2 Two-photon laser uncaging of caged-ATP

We have pursued two different strategies for reaching our goal of mapping feedforward connectivity in a high throughput manner. The first is to use two-photon laser uncaging[81] to focally stimulate individual glomeruli in isolation during a whole cell recording from a lateral horn neuron (Figure 13a). Sequential uncaging in many glomeruli across the antennal lobe would be performed in a single experiment to map out the inputs to a single lateral horn neuron. This strategy is inspired by the success of similar approaches in neocortex[82] and piriform cortex[44].

As a caged compound we decided to use (1-(4,5-dimethoxy-2-nitrophenyl)ethyl)-adenosine triphosphate (DMNPE-caged ATP, Invitrogen and Tocris), in conjunction with exogenous expression of the cation-permeable ATP receptor $P2X_2$. This combination has been used successfully in *Drosophila* for light activation of neurons with single photon

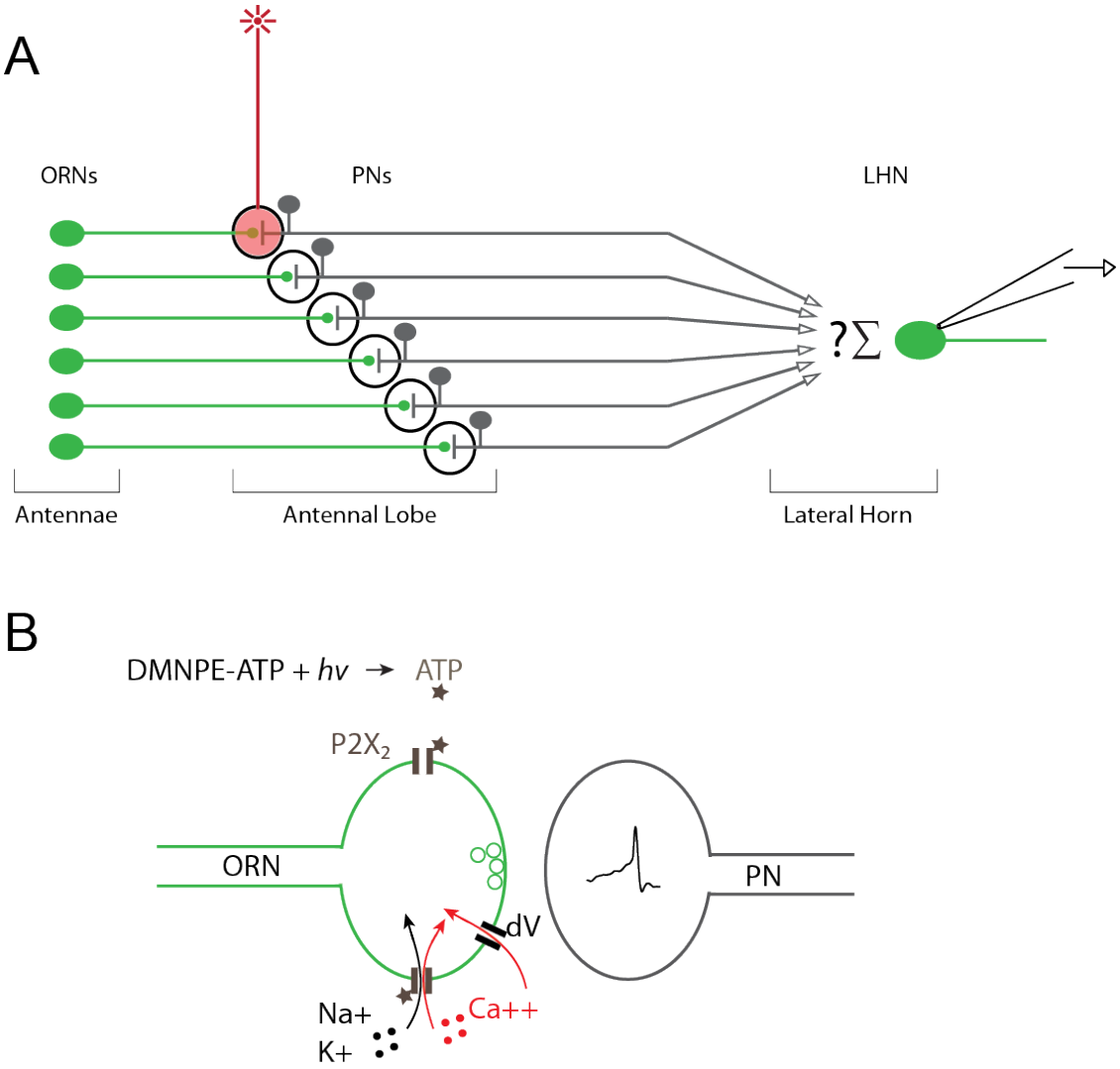

Figure 13. High throughput connectivity mapping

A. Illustration of two-photon laser uncaging strategy to focally stimulate individual glomeruli in isolation during a whole cell recording from a lateral horn neuron. Red laser spot is moved across glomeruli sequentially to test connectivity comprehensively in the antennal lobe.

B. Uncaging strategy in detail. The ATP receptor $P2X_2$ is expressed in olfactory receptor neurons and trafficked to their synaptic terminals. Uncaging of DMNPE-ATP within a glomerulus causes opening of $P2X_2$ and influx of cations including calcium. Either calcium entry through $P2X_2$ or calcium entry through endogenous voltage gated calcium channels leads to neurotransmitter release and PN depolarization.

illumination[83,84]. However, two-photon uncaging of this compound had never been reported. Therefore, our first challenge was to determine if it was feasible to use two-photon excitation to deliver ATP to the brain. We also sought to amplify the response to a potentially small amount of uncaged ATP by expressing the receptor $P2X_2$ in olfactory receptor neurons. $P2X_2$ is trafficked to receptor neuron axon terminals within glomeruli in the antennal lobe. There, channel opening likely leads to two events: Ca^{++} influx through $P2X_2$ itself, and depolarization of the synaptic terminal through $P2X_2$ opening and subsequent opening of endogenous voltage gated calcium channels in the terminal (Figure 13b). This would lead to neurotransmitter release and excitation of PNs projecting to the lateral horn. We reasoned that the high convergence ratio and strength of this synapse[63,85] would lead to amplification of a potentially small uncaging response in the directly responsive neuron to a larger response in the projection neurons.

In order to test this method, we recorded from a PN and filled it with a red dye (Figure 14a). We located the fill and the home glomerulus under two-photon imaging at 800nm, and defined a region of interest (ROI) circumscribed well within the boundaries of the glomerulus. We proceeded to uncage DMNPE-caged ATP with two-photon illumination at 690nm. We raster scanned the ROI for a total illumination duration of 512 ms. We found that under the conditions described in the next paragraph, PNs responded robustly (Figure 14b). We found similar results in several experiments.

There were several important factors in obtaining a strong response from PNs. First, we had to use a high concentration of caged compound to reveal a response (~10mM). Second, we found that the age of the fly affects the expression level of $P2X_2$: young flies under several different conditions revealed weak responses at best. Third, we

found that the preparation type was critical. No responses were obtained in a naked brain (*in vitro*) prep, where olfactory receptor neuron axons are severed and the brain is removed from the head capsule. Fourth, responses were weak unless the caged compound was incubated in a solution containing Apyrase, an adenosine 5'-triphosphatase[86,87]. Early on, we found that washing on caged compound lead to strong depolarizations in PNs, sometimes even leading to temporary depolarization block. We reasoned that this must be due to the presence of free ATP in our batch of caged-ATP. Therefore we pre-incubated our DMNPE-ATP solution with Apyrase (200 units/ml, 37^{o}C, 90 minutes) which should remove free ATP from the solution. This treatment revealed a strong response to uncaging. We conclude that the previous lack of response to uncaging was due to desensitization of $P2X_2$ channels by free ATP[88].

Having arrived at a set of conditions producing robust PN responses to uncaging pulses, we tested the spatial localization of the uncaging mediated response. The previously described parameters define a small volume, but a relatively long duration for uncaging, totaling 512ms. This long window was necessary for generating a large response, but could lead to diffusion of uncaged ATP. This could produce a response in nearby glomeruli, thereby preventing us from achieving the single glomerulus excitation necessary for connectivity mapping. Figure 14c shows results from an experiment where we gradually moved the uncaging ROI laterally, away from the home glomerulus of a recorded PN and found that when the ROI was squarely off the glomerulus, we obtained no response. Therefore two-photon laser uncaging of DMNPE-ATP yields strong and spatially localized excitation of individual glomeruli which can be coupled with whole cell recording of an LHN to attempt connectivity mapping experiments.

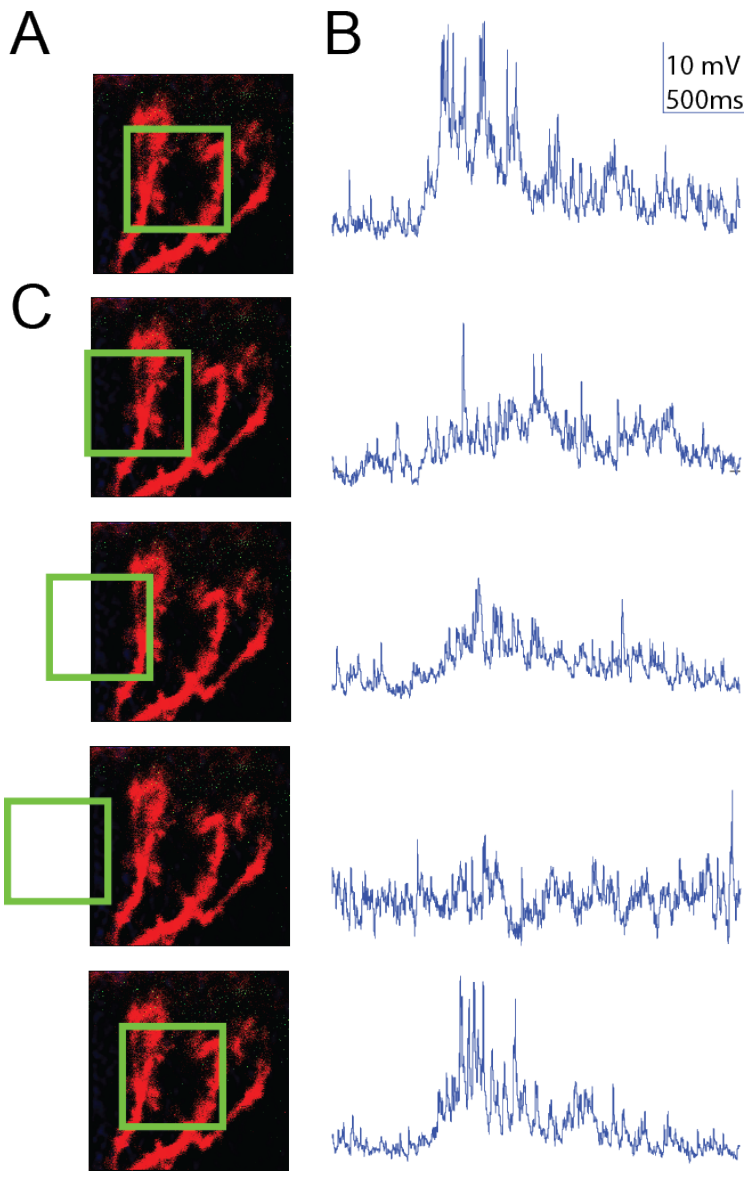

Figure 14. Projection neuron response to two-photon laser uncaging

A. A PN filled with red dye (Alexa Fluor 568) and imaged under two-photon laser scanning microscopy. Green box delineates the field of view used for uncaging DMNPE-ATP.

B. Whole cell current clamp recording obtained from PN displayed in panel a. Trace shows response of PN to uncaging pulse.

C. Gradually moving the uncaging ROI into the adjacent glomerulus leads to loss of PN response

In order to map connectivity across the entire antennal lobe, we need to be able to identify glomeruli, and assign an uncaging ROI for each one. Co-expressing a GFP in olfactory receptor neurons (along with $P2X_2$) provides a good signal that allows the identification of some, especially larger glomeruli. However this signal is not enough to identify the majority of glomeruli as the borders between them become hard to discern for smaller glomeruli. For this purpose, we sought to identify a red vital dye to mark glomerular boundaries in conjunction with the GFP signal present within glomeruli. As glomerular boundaries are relatively glia-rich, we reasoned that Sulforhodamine 101 (SR101), which is used to mark astrocytes in cortical imaging studies[89], would be a good candidate. When injected into the antennal lobe at lower concentrations, we found that this non-toxic dye provides a border signal that demarcates glomeruli (Figure 15).

Two-photon laser uncaging provides a good method for exciting glomeruli individually. However it also presents difficulties. First, it is unclear how many uncaging trials can be performed in one experiment, before sufficient free ATP is generated both through 2P uncaging and spontaneous photolysis over time. At some level of free ATP desensitization will impact response magnitudes significantly. The cost of DMNPE-ATP and the high concentration of compound necessary for eliciting a response dictate a static well for uncaging experiments. Therefore uncaged ATP will not be washed off.

Second, the necessity for using an *in vivo* prep is limiting, in that under such conditions there is significant movement of the brain on both fast and slow timescales. Movement during the experiment could lead to mis-alignment of the actual positions of glomeruli and the ROI coordinates assigned to represent them in three dimensions.

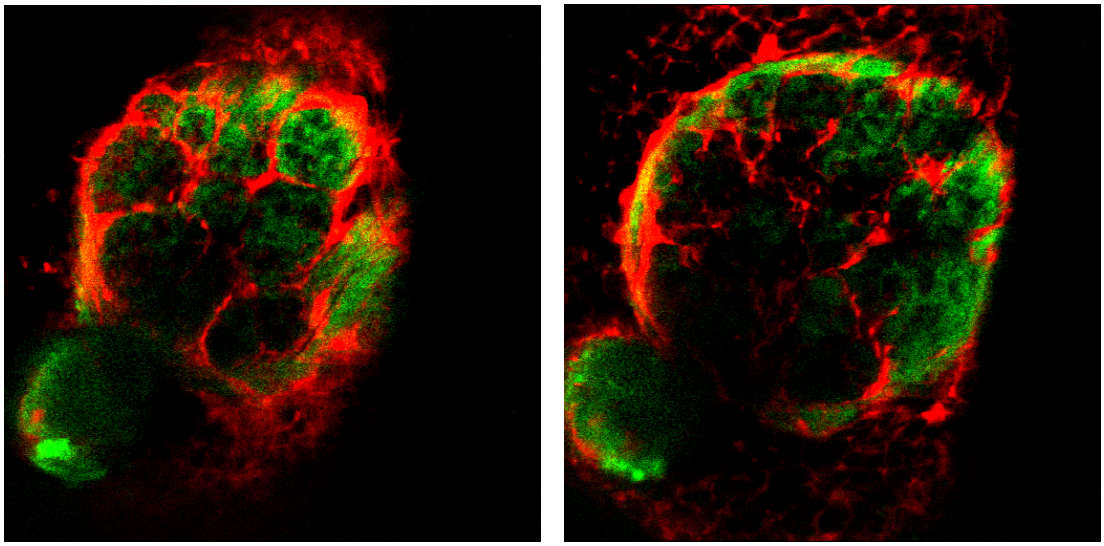

Figure 15. Sulforhodamine 101 provides glomerular boundary signal

Two single z-sections obtained under two-photon microscopy through the antennal lobe. Green signal comes from CD8:GFP expressed by olfactory receptor neurons and red signal is SR101 fluorescence. SR101 was injected into antennal lobe at 100 uM.

Minimizing movement on the micron level is possible but difficult *in vivo*, reducing success rates significantly. Third, the necessity for incubation of the caged compound in an enzyme solution, and the presence of enzyme in the bath add complexity to the experiment.

4.3 Two-photon excitation of light-activated cation channels

Due to the difficulties of the uncaging strategy, we also attempted to use two-photon excitation of a light-activated cation channel to achieve selective excitation of olfactory glomeruli. Channelrhodopsins (ChR) have an amenable two-photon cross section, but very small single channel conductance[90,91]. Therefore the critical issue in two-photon activation of ChR is the number of ChR molecules excited by two-photon illumination. Single glomeruli have a relatively small volume: they can be approximated as spheres of diameter between 5 and 10 micrometers. Furthermore any single type of neuron innervating a glomerulus occupies only a fraction of this space, presenting a small amount of membrane surface area. This led us to attempt the uncaging strategy first. However a recently published[92,93] variant of ChR with a red-shifted excitation spectrum (called ReaChR) was designed and found to have improved membrane trafficking, and presented a potential alternative to the issues described above.

We again expressed ReaChR in olfactory receptor neuron axons to benefit from the amplification inherent in the receptor neuron – projection neuron synapse. In similar experiments to what is shown in figure 14, we found that two-photon excitation of ReaChR is able to produce robust and spatially restricted responses in PNs (Figure 16). The largest responses we obtained with ReaChR expression were substantially larger than

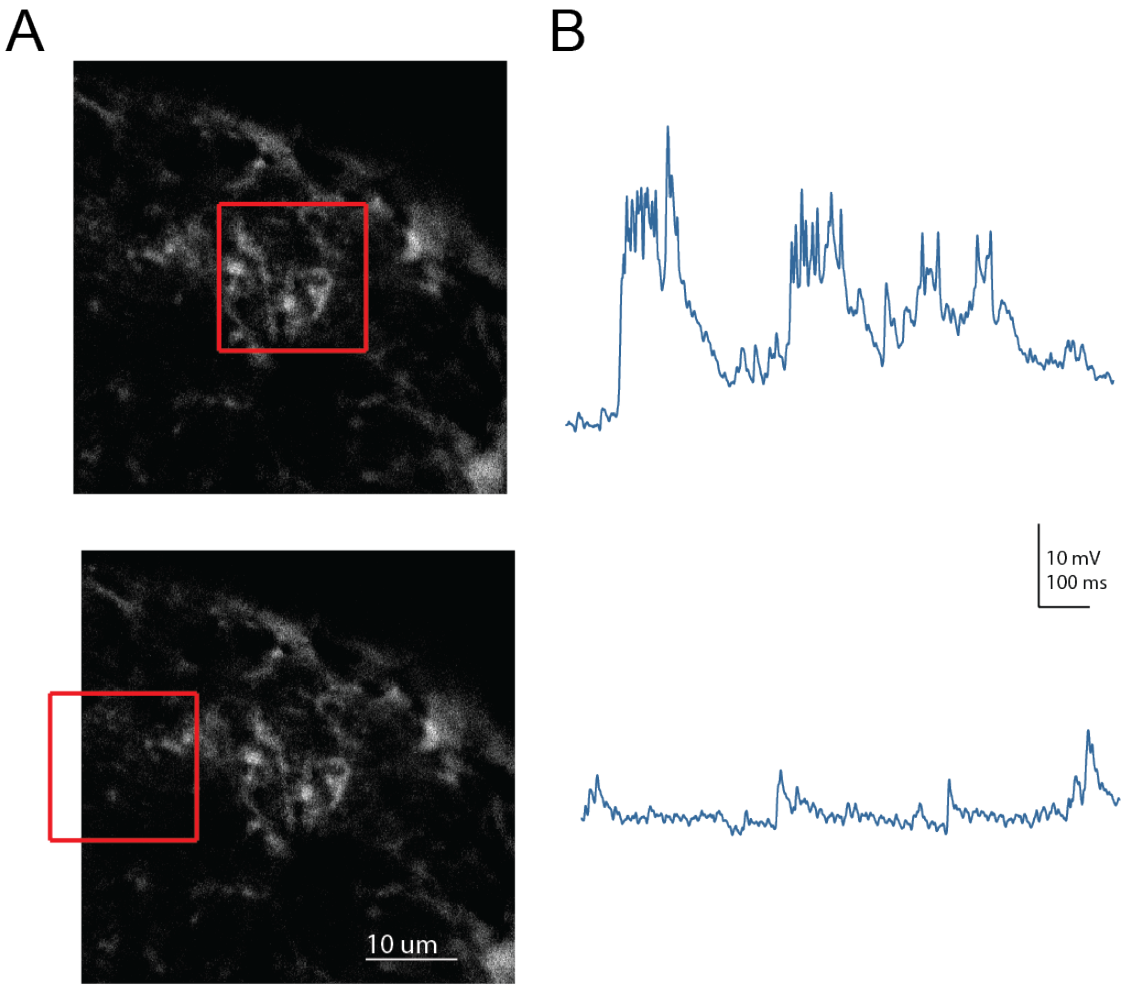

Figure 16. Two photon activation of ReaChR

A. A PN filled with dye (Alexa Fluor 568) and imaged under two-photon laser scanning microscopy. Red box delineates the field of view used for activation of ReaChR.

B. Whole cell current clamp recording obtained from PN displayed in panel a. Trace shows response of PN to illumination at 1000nm within the red box.

those we could obtain with uncaging. Importantly, ReaChR activation worked *in vitro,* even with olfactory receptor neuron axons severed.

This observation indicates that terminals attached to severed axons are still able to depolarize and release transmitter. This raises the following question: why does uncaging fail to work *in vitro* if the terminals are still able to release transmitter? We think the answer lies in the sensitivity of severed axons to the application of trace free ATP present in our caged ATP solution. Enzyme treatment of the caged-ATP solution substantially improves our ability to elicit strong responses *in vivo*, likely through reduction of the free ATP concentration and therefore desensitization. However under the best conditions we reached, we still see some response to wash-in of the enzyme treated caged compound solution. We take this to indicate that we have been unable to remove free ATP completely, and there likely is some $P2X_2$ opening and transmitter release upon wash-in. Despite this, we find that *in vivo*, these conditions yield strong responses. Therefore at least some $P2X_2$ channels must not be desensitized and severed axons must still release transmitter. We reason that the same desensitization conditions must be reached *in vitro*. However we find no response to uncaging. One possible reason is that the transmitter release caused by initial wash-in causes depletion of vesicle pools and the severed axons are much less effective at replenishing them. If this is the case, uncaging would produce $P2X_2$ opening, but no transmitter release. In other words severed axons might be more sensitive to free ATP concentrations and require more aggressive enzyme treatment. We think that further development of the uncaging strategy requires resolution of this issue. Alternatively we could develop a preparation where the brain is dissected out of the head capsule and immobilized, but olfactory receptor neuron axons are not severed.

The ReaChR strategy presents several advantages. First, it allows the use of an *in vitro* preparation much more easily. This makes movement issues significantly easier to solve. Second, there is no desensitization due to free compound and therefore no necessity for pre-incubation. This makes the execution of the experiment easier. In addition, ReaChR activation is likely to provide the opportunity to perform many more trials, potentially obviating the need to identify individual ROIs corresponding to each glomerulus (which takes valuable experimental time). Given sufficient trials, it should be possible to use an un-biased grid like stimulation pattern over the antennal lobe, and to identify the relevant glomeruli post-hoc. Due to these advantages, our plans are to pursue connectivity mapping using ReaChR.

Chapter 5.

Conclusions

In other sensory systems, a neuron's receptive field can be described as a set of positive and negative weights over stimulus space[94] or neural space[95]. Here we show this framework can be extended to higher-order olfactory receptive fields, which are in essence a set of positive and negative weights over olfactory glomeruli. Each glomerulus corresponds to an odorant receptor, and each receptor can be considered selective for a molecular feature or more abstractly, it can be considered selective for a region of odorant stimulus space[4]. Thus, higher-order olfactory receptive fields represent weighted sums of molecular features, or regions of stimulus space.

We find two flavors of higher order olfactory receptive fields. In one type, pooling over strong positive weights leads to a higher order receptive field that is larger in stimulus space in comparison to its inputs. In particular, the case of concentration encoding shows that these receptive fields contain lower resolution information about a larger region of olfactory stimulus space. In the other type we find that weighting strong inputs negatively as well as positively can lead to receptive fields that are smaller in stimulus space in comparison to the excitatory inputs. This more subtraction-like operation likely generates novel selective signals for specific odorants.

In other sensory systems, receptive field structures are non-random, insofar as they have a strong tendency to sample from overlapping regions of stimulus space, reflecting the statistical regularities of the environment[96]. Analogous to this, we have described neurons which sample from glomeruli with overlapping chemical tuning, and we have shown that sampling is highly non-random. We hope that in the near future we

can describe in greater detail the rules of non-random sampling, by mapping feedforward connectivity in a comprehensive and high throughput manner.

Since these neurons are highly stereotyped, we know that every fly devotes significant resources to the computation of similar olfactory signals. It is reasonable to assume that these signals represent stimuli that are ecologically important to the animal. In the more distant future it will be important to investigate how the computations which occur in the lateral horn might relate to the statistical distribution of odors in the environment, their ecological relevance to the organism, and their relationship with particular behavioral programs.

Bibliography

1. Hubel, D. H. & Wiesel, T. N. Receptive fields, binocular interaction and functional architecture in the cat's visual cortex. *J. Physiol.* **160,** 106–154.2 (1962).

2. Clay Reid, R. & Alonso, J.-M. Specificity of monosynaptic connections from thalamus to visual cortex. *Nature* **378,** 281–284 (1995).

3. Priebe, N. J. & Ferster, D. Mechanisms of Neuronal Computation in Mammalian Visual Cortex. *Neuron* **75,** 194–208 (2012).

4. Bargmann, C. I. Comparative chemosensation from receptors to ecology. *Nature* **444,** 295–301 (2006).

5. Araneda, R. C., Kini, A. D. & Firestein, S. The molecular receptive range of an odorant receptor. *Nat. Neurosci.* **3,** 1248–1255 (2000).

6. Dobritsa, A. A., van der Goes van Naters, W., Warr, C. G., Steinbrecht, R. A. & Carlson, J. R. Integrating the molecular and cellular basis of odor coding in the Drosophila antenna. *Neuron* **37,** 827–841 (2003).

7. Hallem, E. A. & Carlson, J. R. Coding of odors by a receptor repertoire. *Cell* **125,** 143–160 (2006).

8. Couto, A., Alenius, M. & Dickson, B. J. Molecular, anatomical, and functional organization of the Drosophila olfactory system. *Curr. Biol. CB* **15,** 1535–1547 (2005).

9. Parnas, M., Lin, A. C., Huetteroth, W. & Miesenböck, G. Odor discrimination in Drosophila: from neural population codes to behavior. *Neuron* **79,** 932–944 (2013).

10. Liang, L. *et al.* GABAergic projection neurons route selective olfactory inputs to specific higher-order neurons. *Neuron* **79,** 917–931 (2013).

11. Tanaka, N. K., Endo, K. & Ito, K. Organization of antennal lobe-associated neurons in adult Drosophila melanogaster brain. *J. Comp. Neurol.* **520,** 4067–4130 (2012).

12. Wang, J. W., Wong, A. M., Flores, J., Vosshall, L. B. & Axel, R. Two-photon calcium imaging reveals an odor-evoked map of activity in the fly brain. *Cell* **112,** 271–282 (2003).

13. Ng, M. *et al.* Transmission of olfactory information between three populations of neurons in the antennal lobe of the fly. *Neuron* **36,** 463–474 (2002).

14. Wilson, R. I., Turner, G. C. & Laurent, G. Transformation of olfactory representations in the Drosophila antennal lobe. *Science* **303,** 366–370 (2004).

15. Kazama, H. & Wilson, R. I. Origins of correlated activity in an olfactory circuit. *Nat. Neurosci.* **12,** 1136–1144 (2009).

16. Olsen, S. R., Bhandawat, V. & Wilson, R. I. Excitatory interactions between olfactory processing channels in the Drosophila antennal lobe. *Neuron* **54,** 89–103 (2007).

17. Olsen, S. R. & Wilson, R. I. Lateral presynaptic inhibition mediates gain control in an olfactory circuit. *Nature* **452,** 956–960 (2008).

18. Olsen, S. R., Bhandawat, V. & Wilson, R. I. Divisive normalization in olfactory population codes. *Neuron* **66,** 287–299 (2010).

19. Yaksi, E. & Wilson, R. I. Electrical coupling between olfactory glomeruli. *Neuron* **67,** 1034–1047 (2010).

20. Wilson, R. I. & Mainen, Z. F. Early Events in Olfactory Processing. *Annu. Rev. Neurosci.* **29,** 163–201 (2006).

21. Tan, J., Savigner, A., Ma, M. & Luo, M. Odor information processing by the olfactory bulb analyzed in gene-targeted mice. *Neuron* **65,** 912–926 (2010).

22. Dhawale, A. K., Hagiwara, A., Bhalla, U. S., Murthy, V. N. & Albeanu, D. F. Non-redundant odor coding by sister mitral cells revealed by light addressable glomeruli in the mouse. *Nat. Neurosci.* **13,** 1404–1412 (2010).

23. Fantana, A. L., Soucy, E. R. & Meister, M. Rat olfactory bulb mitral cells receive sparse glomerular inputs. *Neuron* **59,** 802–814 (2008).

24. Zhu, P., Frank, T. & Friedrich, R. W. Equalization of odor representations by a network of electrically coupled inhibitory interneurons. *Nat. Neurosci.* **16,** 1678–1686 (2013).

25. Kikuta, S., Fletcher, M. L., Homma, R., Yamasoba, T. & Nagayama, S. Odorant response properties of individual neurons in an olfactory glomerular module. *Neuron* **77,** 1122–1135 (2013).

26. Cury, K. M. & Uchida, N. Robust odor coding via inhalation-coupled transient activity in the mammalian olfactory bulb. *Neuron* **68,** 570–585 (2010).

27. Shusterman, R., Smear, M. C., Koulakov, A. A. & Rinberg, D. Precise olfactory responses tile the sniff cycle. *Nat. Neurosci.* **14,** 1039–1044 (2011).

28. Haddad, R. *et al.* Olfactory cortical neurons read out a relative time code in the olfactory bulb. *Nat. Neurosci.* **16,** 949–957 (2013).

29. Smear, M., Shusterman, R., O'Connor, R., Bozza, T. & Rinberg, D. Perception of sniff phase in mouse olfaction. *Nature* **479,** 397–400 (2011).

30. Fukunaga, I., Berning, M., Kollo, M., Schmaltz, A. & Schaefer, A. T. Two distinct channels of olfactory bulb output. *Neuron* **75,** 320–329 (2012).

31. Laurent, G. Olfactory network dynamics and the coding of multidimensional signals. *Nat. Rev. Neurosci.* **3,** 884–895 (2002).

32. Miyamichi, K. *et al.* Cortical representations of olfactory input by trans-synaptic tracing. *Nature* **472,** 191–196 (2011).

33. Sosulski, D. L., Bloom, M. L., Cutforth, T., Axel, R. & Datta, S. R. Distinct representations of olfactory information in different cortical centres. *Nature* **472,** 213–216 (2011).

34. Luo, S. X., Axel, R. & Abbott, L. F. Generating sparse and selective third-order responses in the olfactory system of the fly. *Proc. Natl. Acad. Sci. U. S. A.* **107,** 10713–10718 (2010).

35. Perez-Orive, J. *et al.* Oscillations and sparsening of odor representations in the mushroom body. *Science* **297,** 359–365 (2002).

36. Turner, G. C., Bazhenov, M. & Laurent, G. Olfactory representations by Drosophila mushroom body neurons. *J. Neurophysiol.* **99,** 734–746 (2008).

37. Rennaker, R. L., Chen, C.-F. F., Ruyle, A. M., Sloan, A. M. & Wilson, D. A. Spatial and temporal distribution of odorant-evoked activity in the piriform cortex. *J. Neurosci. Off. J. Soc. Neurosci.* **27,** 1534–1542 (2007).

38. Poo, C. & Isaacson, J. S. Odor representations in olfactory cortex: 'sparse' coding, global inhibition, and oscillations. *Neuron* **62,** 850–861 (2009).

39. Miura, K., Mainen, Z. F. & Uchida, N. Odor representations in olfactory cortex: distributed rate coding and decorrelated population activity. *Neuron* **74,** 1087–1098 (2012).

40. Honegger, K. S., Campbell, R. A. A. & Turner, G. C. Cellular-resolution population imaging reveals robust sparse coding in the Drosophila mushroom body. *J. Neurosci. Off. J. Soc. Neurosci.* **31,** 11772–11785 (2011).

41. Apicella, A., Yuan, Q., Scanziani, M. & Isaacson, J. S. Pyramidal cells in piriform cortex receive convergent input from distinct olfactory bulb glomeruli. *J. Neurosci. Off. J. Soc. Neurosci.* **30,** 14255–14260 (2010).

42. Caron, S. J. C., Ruta, V., Abbott, L. F. & Axel, R. Random convergence of olfactory inputs in the Drosophila mushroom body. *Nature* **497,** 113–117 (2013).

43. Gruntman, E. & Turner, G. C. Integration of the olfactory code across dendritic claws of single mushroom body neurons. *Nat. Neurosci.* **16,** 1821–1829 (2013).

44. Davison, I. G. & Ehlers, M. D. Neural circuit mechanisms for pattern detection and feature combination in olfactory cortex. *Neuron* **70,** 82–94 (2011).

45. Franks, K. M. *et al.* Recurrent circuitry dynamically shapes the activation of piriform cortex. *Neuron* **72,** 49–56 (2011).

46. Poo, C. & Isaacson, J. S. A major role for intracortical circuits in the strength and tuning of odor-evoked excitation in olfactory cortex. *Neuron* **72,** 41–48 (2011).

47. Papadopoulou, M., Cassenaer, S., Nowotny, T. & Laurent, G. Normalization for sparse encoding of odors by a wide-field interneuron. *Science* **332,** 721–725 (2011).

48. Tanaka, N. K., Awasaki, T., Shimada, T. & Ito, K. Integration of chemosensory pathways in the Drosophila second-order olfactory centers. *Curr. Biol. CB* **14,** 449–457 (2004).

49. Murthy, M., Fiete, I. & Laurent, G. Testing odor response stereotypy in the Drosophila mushroom body. *Neuron* **59,** 1009–1023 (2008).

50. De Belle, J. S. & Heisenberg, M. Associative odor learning in Drosophila abolished by chemical ablation of mushroom bodies. *Science* **263,** 692–695 (1994).

51. Dubnau, J., Grady, L., Kitamoto, T. & Tully, T. Disruption of neurotransmission in Drosophila mushroom body blocks retrieval but not acquisition of memory. *Nature* **411,** 476–480 (2001).

52. Heimbeck, G., Bugnon, V., Gendre, N., Keller, A. & Stocker, R. F. A central neural circuit for experience-independent olfactory and courtship behavior in Drosophila melanogaster. *Proc. Natl. Acad. Sci. U. S. A.* **98,** 15336–15341 (2001).

53. Jefferis, G. S. X. E. *et al.* Comprehensive maps of Drosophila higher olfactory centers: spatially segregated fruit and pheromone representation. *Cell* **128,** 1187–1203 (2007).

54. Stocker, R. F., Lienhard, M. C., Borst, A. & Fischbach, K. F. Neuronal architecture of the antennal lobe in Drosophila melanogaster. *Cell Tissue Res.* **262,** 9–34 (1990).

55. Ruta, V. *et al.* A dimorphic pheromone circuit in Drosophila from sensory input to descending output. *Nature* **468,** 686–690 (2010).

56. Gupta, N. & Stopfer, M. Functional analysis of a higher olfactory center, the lateral horn. *J. Neurosci. Off. J. Soc. Neurosci.* **32,** 8138–8148 (2012).

57. Stensmyr, M. C., Giordano, E., Balloi, A., Angioy, A.-M. & Hansson, B. S. Novel natural ligands for Drosophila olfactory receptor neurones. *J. Exp. Biol.* **206,** 715–724 (2003).

58. Sweeney, L. B. *et al.* Temporal Target Restriction of Olfactory Receptor Neurons by Semaphorin-1a/PlexinA-Mediated Axon-Axon Interactions. *Neuron* **53,** 185–200 (2007).

59. Pfeiffer, B. D. *et al.* Tools for neuroanatomy and neurogenetics in Drosophila. *Proc. Natl. Acad. Sci. U. S. A.* **105,** 9715–9720 (2008).

60. Wilson, R. I. & Laurent, G. Role of GABAergic inhibition in shaping odor-evoked spatiotemporal patterns in the Drosophila antennal lobe. *J. Neurosci. Off. J. Soc. Neurosci.* **25,** 9069–9079 (2005).

61. Manseau, L. *et al.* GAL4 enhancer traps expressed in the embryo, larval brain, imaginal discs, and ovary of Drosophila. *Dev. Dyn. Off. Publ. Am. Assoc. Anat.* **209,** 310–322 (1997).

62. Stocker, R. F., Heimbeck, G., Gendre, N. & de Belle, J. S. Neuroblast ablation in Drosophila P[GAL4] lines reveals origins of olfactory interneurons. *J. Neurobiol.* **32,** 443–456 (1997).

63. Kazama, H. & Wilson, R. I. Homeostatic matching and nonlinear amplification at identified central synapses. *Neuron* **58,** 401–413 (2008).

64. Larsson, M. C. *et al.* Or83b encodes a broadly expressed odorant receptor essential for Drosophila olfaction. *Neuron* **43,** 703–714 (2004).

65. Ai, M. *et al.* Acid sensing by the Drosophila olfactory system. *Nature* **468,** 691–695 (2010).

66. Tuthill, J. C., Nern, A., Holtz, S. L., Rubin, G. M. & Reiser, M. B. Contributions of the 12 neuron classes in the fly lamina to motion vision. *Neuron* **79,** 128–140 (2013).

67. Patterson, G. H. & Lippincott-Schwartz, J. A photoactivatable GFP for selective photolabeling of proteins and cells. *Science* **297,** 1873–1877 (2002).

68. Datta, S. R. *et al.* The Drosophila pheromone cVA activates a sexually dimorphic neural circuit. *Nature* **452,** 473–477 (2008).

69. Pologruto, T. A., Sabatini, B. L. & Svoboda, K. ScanImage: flexible software for operating laser scanning microscopes. *Biomed. Eng. Online* **2,** 13 (2003).

70. De Bruyne, M., Foster, K. & Carlson, J. R. Odor coding in the Drosophila antenna. *Neuron* **30,** 537–552 (2001).

71. Silbering, A. F. *et al.* Complementary function and integrated wiring of the evolutionarily distinct Drosophila olfactory subsystems. *J. Neurosci. Off. J. Soc. Neurosci.* **31,** 13357–13375 (2011).

72. Jefferis, G. S., Marin, E. C., Stocker, R. F. & Luo, L. Target neuron prespecification in the olfactory map of Drosophila. *Nature* **414,** 204–208 (2001).

73. Jefferis, G. S. X. E. *et al.* Developmental origin of wiring specificity in the olfactory system of Drosophila. *Dev. Camb. Engl.* **131,** 117–130 (2004).

74. Marin, E. C., Jefferis, G. S. X. E., Komiyama, T., Zhu, H. & Luo, L. Representation of the glomerular olfactory map in the Drosophila brain. *Cell* **109,** 243–255 (2002).

75. Wong, A. M., Wang, J. W. & Axel, R. Spatial representation of the glomerular map in the Drosophila protocerebrum. *Cell* **109,** 229–241 (2002).

76. Lin, H.-H., Lai, J. S.-Y., Chin, A.-L., Chen, Y.-C. & Chiang, A.-S. A map of olfactory representation in the Drosophila mushroom body. *Cell* **128,** 1205–1217 (2007).

77. Kreher, S. A., Mathew, D., Kim, J. & Carlson, J. R. Translation of sensory input into behavioral output via an olfactory system. *Neuron* **59,** 110–124 (2008).

78. Asahina, K., Louis, M., Piccinotti, S. & Vosshall, L. B. A circuit supporting concentration-invariant odor perception in Drosophila. *J. Biol.* **8,** 9 (2009).

79. Borst, A. Computation of olfactory signals inDrosophila melanogaster. *J. Comp. Physiol.* **152,** 373–383 (1983).

80. Geisler, C. D. *From Sound to Synapse: Physiology of the Mammalian Ear*. (Oxford University Press, 1998).

81. Denk, W. Two-photon scanning photochemical microscopy: mapping ligand-gated ion channel distributions. *Proc. Natl. Acad. Sci.* **91,** 6629–6633 (1994).

82. Yoshimura, Y., Dantzker, J. L. & Callaway, E. M. Excitatory cortical neurons form fine-scale functional networks. *Nature* **433,** 868–873 (2005).

83. Zemelman, B. V., Nesnas, N., Lee, G. A. & Miesenbock, G. Photochemical gating of heterologous ion channels: remote control over genetically designated populations of neurons. *Proc. Natl. Acad. Sci. U. S. A.* **100,** 1352–1357 (2003).

84. Lima, S. Q. & Miesenböck, G. Remote control of behavior through genetically targeted photostimulation of neurons. *Cell* **121,** 141–152 (2005).

85. Bhandawat, V., Olsen, S. R., Gouwens, N. W., Schlief, M. L. & Wilson, R. I. Sensory processing in the Drosophila antennal lobe increases reliability and separability of ensemble odor representations. *Nat. Neurosci.* **10,** 1474–1482 (2007).

86. Kettlun, A. M. *et al.* Properties of two apyrases from Solanum tuberosum. *Phytochemistry* **21,** 551–558 (1982).

87. Bianco, F. *et al.* Different properties of P2X7 receptor in hippocampal and cortical astrocytes. *Purinergic Signal.* **5,** 233–240 (2009).

88. Ding, S. & Sachs, F. Inactivation of P2X2 purinoceptors by divalent cations. *J. Physiol.* **522,** 199–214 (2000).

89. Nimmerjahn, A., Kirchhoff, F., Kerr, J. N. & Helmchen, F. Sulforhodamine 101 as a specific marker of astroglia in the neocortex in vivo. *Nat. Methods* **1,** 31–37 (2004).

90. Rickgauer, J. P. & Tank, D. W. Two-photon excitation of channelrhodopsin-2 at saturation. *Proc. Natl. Acad. Sci. U. S. A.* **106,** 15025–15030 (2009).

91. Feldbauer, K. *et al.* Channelrhodopsin-2 is a leaky proton pump. *Proc. Natl. Acad. Sci. U. S. A.* **106,** 12317–12322 (2009).

92. Lin, J. Y., Knutsen, P. M., Muller, A., Kleinfeld, D. & Tsien, R. Y. ReaChR: a red-shifted variant of channelrhodopsin enables deep transcranial optogenetic excitation. *Nat. Neurosci.* **16,** 1499–1508 (2013).

93. Inagaki, H. K. *et al.* Optogenetic control of Drosophila using a red-shifted channelrhodopsin reveals experience-dependent influences on courtship. *Nat. Methods* **11,** 325–332 (2014).

94. Dayan, P. & Abbott, L. F. *Theoretical neuroscience computational and mathematical modeling of neural systems*. (Massachusetts Institute of Technology Press, 2001).

95. Rust, N. C., Mante, V., Simoncelli, E. P. & Movshon, J. A. How MT cells analyze the motion of visual patterns. *Nat. Neurosci.* **9,** 1421–1431 (2006).

96. Simoncelli, E. P. Vision and the statistics of the visual environment. *Curr. Opin. Neurobiol.* **13,** 144–149 (2003).